Life Cycle Assessment Study on Luminescent Solar Concentrators

Jelmer Dijkstra, 3360954

Supervisors:
A. Louwen (MSc)
Dr. W.G.J.H.M. van Sark

2^{nd} reader:
Dr. E. Nieuwlaar

Master: Sustainable Development
Track: Energy and Resources
University of Utrecht
Netherlands
July 24, 2015

Abstract

In order to make a transition towards a larger share of renewables in the global electricity generation, several renewable sources can be utilized. One of these sources is the sun. Photovoltaic panels already are capable of converting this source to electricity with efficiencies of 15 to 20% in an economically viable way. However, some downsides can be attributed to these conventional panels and that is the reason why research has also focussed on other types of photovoltaic cells. One of these are luminescent solar concentrators. This is not a completely new technology, but recently interest has sparked again due to the lowering in prices of PV panels and the increase in price of fossil fuels. In this thesis a Life Cycle Assessment study on building integrated luminescent solar concentrators has been performed. First, a literature study has been conducted to see what the current state of the technology of the luminescent solar panels is. Second, an inventory of materials required to produce luminescent solar concentrator modules is provided. Then, the modules had their impact assessed by the use of the Ecoinvent database. From this, both the CO_2-eq/kWh as the CED and EPBT are derived. These results are then used to compare luminescent solar concentrators with conventional PV and other building materials. In this study it is found that the best modules that are available can have an EPBT as low as 5 years, but the CO_2-eq/kWh is high compared to conventional PV. Furthermore, some considerations for installing these modules and future research topics are suggested.

Contents

Chapter 1

Introduction

Currently most of the electricity is produced by conversion of fossil resources in power plants. A fraction is produced from renewable sources such as wind, solar and water. In 2012, 21.2% was produced from renewable sources, 10.9% from nuclear sources and 67.9% from fossil resources (IEA, 2014). In the last few decades, various scientist and environmental organisations have been warning for the negative effects of using fossil resources. The linked greenhouse gasses (GHG) emissions cause the solar radiation from the sun to be trapped in the atmosphere when reflected from the earth's surface which results in a rise of the average global temperature and this influences e.g. the global weather patterns as well as the sea level (IPCC, 2014). It is therefore argued that more research and investment should go towards renewable energy and GHG emissions should decrease as soon as possible. In the most optimistic scenario, a maximum average temperature rise of 2° C can be achieved, but at current emission rates 5° C is more realistic according to the IPCC reports (IPCC, 2014). Many governmental bodies have set ambitious targets to increase the share of renewable energy in their countries to become less dependent on the imports of fossil resources and decrease the GHG intensity of their economy, e.g. the 2020 goals of the European Union ("Europe 2020", 2015). It is argued that there is not one perfect renewable source available and a broad spectrum of renewables have to be adopted in order to achieve these targets.

One of the available renewable energy sources is solar energy. The energy falling from the sun on the earth's surface per year is enormous in comparison with our annual consumption. Harvesting a fraction of this energy thus provides a great opportunity of changing our electricity production patterns towards a more sustainable situation. The conversion of solar energy to electricity has already been discovered in the 19th century based on selenium, however conversion efficiencies were very low, at which point scientists believed that photovoltaic (PV) cells did not have any future. However after new theoretical evidence from Albert Einstein and an accidental discovery of the electric properties of silicon, researchers from Bell labs invented a solar cell that was 50 times as efficient as the previous selenium was 20 years earlier. This lead to a solar cell with 6%

efficiency (Chapin et al., 1954). This lead to a revival of interest in PVs and modules and efficiencies have improved ever since. Other types of PV cells have also been invented e.g. GaAs based cells and organic dyed cells, although silicon based PV remains the most developed.

In the last decade, the installation rates of PV panels have grown worldwide due to various subsidies and policies (Van Sark et al., 2014). The fast growth of installation rates is also caused by the lowering in prices, though the panels still face competition with fossil fuels. However, the downside of the widely applied silicon PV-panels is their limited applicability due to their fixed design. They are limited in shape, often relative heavy in weight and can be either placed on the roof or in large open fields. Another downside is that they operate best in direct sunlight which also limits their applicability in the building industry. These are some of the many reasons why research has also focused on other types of solar cells. One of the types of solar cells that have seen increased interest from research groups around the world are luminescent solar concentrators (LSCs). They work in a slightly different way compared to other more conventional PV-panels however due to their non-fixed shape and other unique features they can have applications in areas where conventional PV is not possible or feasible. Building integration of these LSCs is one aspect that makes them attractive. As the modules are semi-transparant and come in a variety of colours, architects and building manufacturers might be interested to decorate their buildings with these modules. They can be integrated into the building-façade, could replace regular window frames, and can be placed on the roof to enhance the natural lightening in e.g. hallways. Other benefits of LSCs are that they have a large low-cost area which is combined with a small expensive PV cell resulting in a maximum potential for their price to area relation. One way to assess the impact of PV modules is to perform a life cycle assessment study. This term has been coined in 1990, and is currently an accepted standard to assess impacts of nearly all products and processes. Publications in this field are many on an annual basis. A life cycle assessment study will also be the core of this thesis. This study aims to answer the following research question to provide arguments for the consideration of LSCs in the building environment:

- What is the environmental impact of LSCs.

Chapter 2

Outline of the thesis

First a short description of the operational principles of LSCs is provided, explaining the current state of the research in this field, and providing the reader insight into the subject prior to the actual research. In this section, the different components that make up the LSC, as well as the different losses and limitations that can occur during the conversion process are touched upon by conducting a literature study.

Second, the environmental impact of the LSCs is assessed. This is done through a Life Cycle Assessment (LCA) study. At the end of this section the different impacts are compared and analysed for a selection of modules and configurations. The aim is to be able to give a comparison between building integrated LSCs and other building integrated types of PVs, there for a literature study has to be conducted to find other LCA studies that have found impacts for these other types of PVs. Then a conclusion can be drawn on how much the impact is for LSCs and these results can be discussed in comparison with other systems to put a value on the environmental impact from the electricity generation by both types of PV.

Finally, the previous step is summarized and the results are presented to answer the research question, while also performing a sensitivity and uncertainty analysis to critically review the results.

Chapter 3

Introduction to LSCs

In order to get an idea of the progress and problems faced in the LSC field an overview is given based on a review paper by Debije (Debije et al., 2012). LSCs are sheets of transparent material or waveguides that harvest solar radiation. These sheets are then dyed by luminescent particles (luminophores) such as organic dyes and quantum dots. These particles are designed to convert the wavelength of the incoming solar radiation to another wavelength that matches the optimal wavelength of the solar cells that are attached to the sides of these sheets and the concentrated bundle of radiation causes these cells to work at close their maximum potential (Figure 3.1).

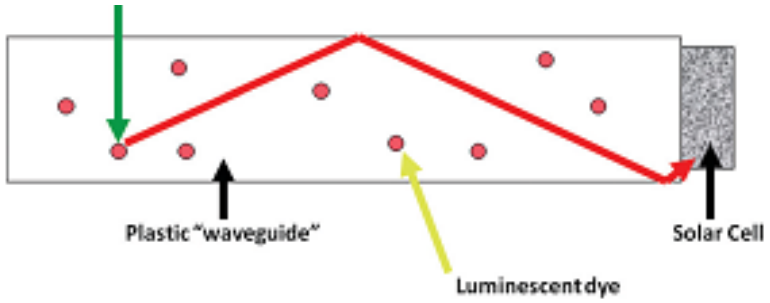

Figure 3.1: Visualisation of the working principal of LSCs, green arrow illustrates the incoming solar radiation and the red arrow illustrates the movement through the waveguide towards the solar cell (Debije et al, 2012).

Thus they work by harvesting light with a large area of transparent dyed material and converting and transporting this light towards the side of the cell where it is converted to electricity. The increased optical efficiency is a result of various processes that are happening inside the LSC, e.g. how light particles interact with the luminescent molecules and what fraction of light is trapped inside the LSC due to internal reflection. The product of all these processes is what is used to calculate the final optical efficiency of the LSC (Equation 3.1).

Losses can occur in all these processes and research is still conducted on how to minimize these losses. Each term in equation 1 can be coupled to one of these losses. Some of the losses are visualized in Figure 3.2. Another loss is not caused in the LSC but rather during the conversion to electricity in the solar cell attached to the side, this is loss 4 in Figure 3.2.

$$\eta_{opt} = (1 - R)P_{TIR} \times \eta_{abs} \times \eta_{PLQY} \times \eta_{Stokes} \times \eta_{host} \times \eta_{TIR} \times \eta_{self} \quad (3.1)$$

R = Reflection of solar light from the waveguide surface (5a).

$\mathbf{P}_{TIR}$ = Total internal reflection efficiency (1).

η_{abs} = Fraction of solar light absorbed by the dye (3a, 3b).

η_{PLQY} = Photo luminescent quantum yield of the used luminophores (3c).

η_{Stokes} = Energy lost due to heat generation during absorption and emission event (3c).

η_{host} = Transport efficiency of the waveguide photons through the waveguide (5b, 5c).

η_{TIR} = Internal reflection efficiency determined by the smoothness of the surface (5d).

η_{self} = Transport efficiency of the waveguide photons related to re-absorption of these photons by another luminophore (2).

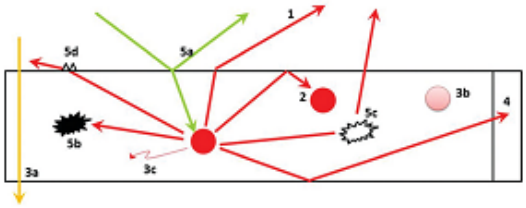

Figure 3.2: Illustration showing loss mechanisms occurring in LSCs (Debije et al, 2012)

The absorption and re-emission of photons in LSCs changes the entropy of the system. The maximum concentration that can be achieved by LSCs is linked to the heat generation during these events, and thus from the Stokes shift of the luminescent molecules. Stokes shift is the wavelength separation between the peak of the most red-shifted absorption band and the most blue-shifted emission band. For example, a luminophore with a Stokes shift of 0.2 eV the max concentration is approximately 2000 times (Equation 3.2).

$$C \approx \frac{e_2^3}{e_1^3} \exp \frac{e_1 - e_2}{\kappa T_0} \tag{3.2}$$

$\mathbf{e}_2$ / $\mathbf{e}_1$ = Photon energies of emitted and absorbed photons, respectively.

κ = Boltzmann's constant.

$\mathbf{T}_0$ = Ambient temperature.

Equation 3.1 can be used to explain the different losses that can occur in the LSCs. A short summary of the causes and consequences is given as this gives an idea of the problems that future research will have to tackle to increase the efficiency of LSCs and improve the electricity output.

3.1 Surface losses (R) and internal reflection efficiency ($\mathbf{P}_{TIR}$)

Regarding surface losses it is estimated that 50 to 70% of the photons entering the waveguide is reflected outside again and this is the key loss in a LSC. Research has tried to reduce these losses by two main processes, aligning the luminophores and by the application of selective mirrors. *Aligning* the luminophores can be achieved through using self-aligning nanorods or using a host material that can be stretched to achieve the specific alignment required or mixing in a host that can be spontaneously aligned, such as liquid crystals. However changing the alignment of the luminophores also affects the absorption efficiency. An ideal alignment would combine both the reduced surface losses from the vertical alignment with the enhanced emission directions of the horizontal alignment by applying the luminophores in a tilted alignment. Currently this has not been achieved with perfect results. Using *selective mirrors* surface losses can also be reduced. Several top layers have been suggested and studied on, such as wavelength selective mirrors that allow incoming light to enter the waveguide but to be reflective for emitted wavelengths from the luminophore. Reduction of 20 to 30% have been achieved resulting in a 12% efficiency improvement.

3.2 Re-absorption events (η_{self})

Re-absorption of emitted photons by other luminophores is a result from the often limited Stokes shift. Emitted photons are likely to be re-absorbed by other luminophores encountered while moving through the waveguide. Sometimes the absorbed photon is emitted in a way that allows to escape the waveguide or the absorbed photon is not emitted due to non-radiative relaxation (heat). One way to tackle this problem is by developing luminophores with a larger

Stokes shift. Another solution is to implement a dopant in the waveguide that can alter the electronic state around the luminophores thereby increasing the Stokes shift as well. It is also possible to stack several waveguides containing different types of luminophores and putting the most efficient ones on top. By doing this the emitted photons do not encounter another lower efficiency luminophore and radiation escaping the waveguide has a chance of encountering another luminophore in an adjacent layer. It is also possible to concentrate the luminophores in a thin layer on the sides of the waveguide so that there is only a chance of absorption at each time of internal reflection. A downside is that some luminophores have limited solubility which results in an underperformance of the thin layers. This technique would have benefits during production, since it is very easy to apply large areas of luminescent layers on top of waveguide material. Other solutions suggest to physically separate layers of waveguides with a thin film of waveguides that are empty to reduce the number of encounters while being internally reflected in the waveguide, and using lenses to concentrate the incoming radiation on specific patterns of dyes.

3.3 Luminophores (η_{abs} / η_{self}) and their yield (η_{PLQY} / η_{Stokes})

Luminophores can be divided into three categories. These categories are organic dyes, quantum dots and rare earth ions. Each type has different characteristics and these are discussed per category:

Organic dyes

- Consist of π-bonds.
- Main absorption wavelength (λ_{abs}) mainly determined by chain length and number of π-electrons in the conjugated plane.
- Restrictions: Limited breadth of spectral absorptions and limited photostability.
- Solutions: Synthesising more resistant molecules or applying UV-absorbing layer.

Quantum Dots (QDs)

- Small sized (10-100 nm) particles consisting of semiconducting materials.
- Absorption threshold can be tuned by varying particle size.
- More stable compared to organic-based counterparts.
- Restrictions: Sensitivity to oxygen and light when outside a solid matrix and uncertainty regarding their toxicity in the chemical composition and processing conditions

- Solutions: Research aims to reduce threats by looking into jelly dots and safer materials such as silicon.

Rare earth ions

- Show promising absorptions in the infra-red and UV region.
- Restrictions: Show low quantum conversion efficiencies.
- Solutions: Combine two types of ions into one LSC or to combine ions with ligand complexes.

Luminophores themselves while absorbing and admitting radiation can also cause losses if they cause non-radiative emissions or have a Stokes shift that is not broad enough. A good luminophore must therefore contain the following characteristics:

- Broad spectral absorption.
- High absorption efficiency over the whole absorption spectrum.
- Large Stokes shift.
- High luminescent efficiency.
- Matching the emitted photons to the spectral response of the PV-cell.
- Solubility in the host matrix material.

3.4 Waveguide losses (η_{host} / η_{TIR})

Waveguide losses occur at several moments. Initially there is 4% of the incident light that is reflected from the waveguide surface. This can be solved with regular anti-reflective coatings, however this would not be much of a help since the internal reflection of LSCs depends on a smooth surface area and adding an anti-reflective coating often does not result in a smooth surface. Waveguides should also be dust and scratch free. Another option is to increase the size of a LSC. This would reduce the cost of installation, however this often results in a reduced output due to the increased re-absorption by other luminophores and by the waveguide material itself. One would also prefer to use luminophores with near infra-red emissions but the waveguide material is not stable under these conditions thus resulting in increased degradation of the waveguide. Alternative materials for waveguides have been studied that are more flexible or have a higher refractive index. It is also found that changing the shape often increases the efficiency by a small amount, but this is not enough to allow for the increased production costs.

3.5 Photovoltaic cell

Photovoltaic losses occurring are related with the specific band-gap of silicon-based PV of around 1.1 eV. Photons with higher energies are still converted but the excessive energy is converted to heat and a warming of the PV unit results in lower performance. For smaller wavelengths, this band gap results in a lower response of the attached cell. The advantage of LSCs in this case is that they often emit a narrow range of wavelengths centred around red and near infra-red wavelengths (maximum of 720 nm), giving as an advantage that the PV cell should remain cool under normal operating conditions. It may be possible to tune the radiation emitted by the luminophores with the spectral response of the solar cell. Another option to increase the efficiency is to shift to other types of solar cells based on GaAs and InGaP, however these cells currently cannot be produced economically thus the more economic option is preferred.

3.6 Concluding remarks

Above summary of the current status on the research on LSCs shows that research has progressed and various solutions are found and suggested to tackle certain efficiency losses. The perfect LSC does not yet exist, however average efficiencies are starting to reach 5%.

Chapter 4

LCA on LSCs

The LCA study will be conducted according to the ISO 14040 and ISO 14044 guidelines. Following these guidelines helps the policy makers and other parties in applying the results in their business decisions where the most sustainable solutions are preferred, or a comparison based on specific factors is desired. The LCA will be an attributional LCA study which aims to determine the environmental impact from the fabrication and application of building integrated LSCs starting from the raw material extraction through the various processing steps ending with the disposal of the module through either recycling or other end-of-life methods. Next to an attributional LCA a consequential LCA approach is also available which determines how industrial or political changes and decisions can change the environmental flows required for products however for this specific study an attributional approach is preferred. After the materials and associated emissions are known, the lifetime emissions of the modules are compared with conventional PV modules. The guidelines describing the phases are:

1. Goal and Scope definition.
2. Life Cycle Inventory Analysis (LCI).
3. Life Cycle Impact Assessment (LCIA).
4. Interpretation.

4.1 Goal and Scope definition.

The goal of the LCA study is to determine the environmental impact from LSCs manufacturing, installation, operation and disposal steps in terms of GHG emissions that are emitted during the aforementioned steps. The perspective used is a cradle-to-grave perspective. All the GHG emissions are expressed in the amount of CO_2 equivalents (CO_2-eq)/kWh. Next to the GHG emissions, the cumulative energy demand (CED) and the energy payback time (EPBT) are calculated. These values are commonly used in LCA studies focussing on conventional PV modules therefore a comparison can be made with the different PV options that are currently available. The functional unit of this LCA will be a kWh electricity that is generated by a BIPV module. For the GHG emissions this means that the comparison is based on CO_2-eq, thus the CO_2 intensity of the electricity produced by a BIPV module. In the case of CED, the total amount of energy required to produce a BIPV module including the BOS components are calculated. This is expressed as primary energy in MJ per m^2 of module area, from both the incorporated materials and the manufacturing steps. Since different types of PV have different conversion efficiencies it is advised to use the CED/kWp ratio (Laleman et al., 2013). The EPBT is calculated by dividing the total primary energy that is required for the complete BIPV module production (including the BOS components) with the annual primary energy savings that are achieved by the electricity production of the module (Equation 4.1). For this the amount of energy produced in kWh has to be converted to the amount of primary energy that would otherwise have been used in the electricity industry, based on the electricity mix in a specific country.

$$EPBT = \frac{E_{input} + E_{bos}}{E_{output}} \tag{4.1}$$

The aforementioned scope of this LCA study is thus the cradle-to-grave process of the production of a building integrated LSC module. This starts with the primary resource extraction and processing to the manufacturing of the components of the LSC which are then assembled and combined with the BOS components to produce an installable LSC unit. After a certain timespan the LSC unit is either recycled or disposed. Due to the limited experience in the field of LSC on mass production on an industrial scale it is assumed that the processes used are similar to other commonly used practices in industry such as chemical processes from the chemical industry, plastic moulding and casting from the plastic industry and fabrication similar to other fabrication techniques used in the PV industry. It could be that certain processes have a multi-output of which one product is used in the LSC module. If this is the case then a clear distinction has to be made on how the energy required should be divided. In this study it is chosen to look at the mass of the outputs that is realized in such processes.

4.2 Life Cycle Inventory Analysis (LCI)

In order to determine the environmental impacts from the production of LSCs first the different production pathways relevant for the materials required for the final LSCs product have to be determined. Once the production pathways of these major components are known, the assembling of the complete LSC module is looked into. The products required prior to the assembly stage of the LSC can be split into different subcategories, similar to the different components that make up the LSC:

- Waveguide material
- Luminophores
- Photovoltaic cell

With these three components the primary LSC module can be build. Once this process is complete, the only step left to end up with a complete LSC module is the attachment of the BOS components and the implementing in a final framework fit for building integration. These follow up steps are:

- Waveguide and luminophore mixing and casting
- Combining LSC sheet with photovoltaic unit on one or multiple sides.
- Combining with BOS components and building final framework.

In this LCI the different production pathways for the primary components will be explained and the follow up steps required for the LSC production are discussed. The components will be discussed per category rather than per LSC for the sake of clarity since the final assembling will be similar for each different type of LSC, the only difference being the primary components.

4.2.1 Waveguide material

The different waveguide materials available all have similar physical properties. They have diffraction indexes similar to glass and can be drop casted or injection moulded into different shapes required for their final application. In the case of LSCs, this is often achieved by casting between two plates of glass or metal with a spacer to achieve the required thickness. After the casting process the plates can be cut to the specific size that is demanded. Different waveguide materials are used in the current research field and the pathways to produce these from primary products is explained.

Polycarbonate (PC)

PC is a polymer that is manufactured in large quantities. Several reaction pathways for the production of PC exist and most rely on the use of Bisphenol A (BPA). In many of the research papers on LSCs it is not specified what the

specific structure of the PC used is as only the manufacturer from which the PC is obtained is specified, but most pathways use BPA. Often another product, phosgene is used but methods without this product do exist and are favoured for being more environmentally friendly. However most PC is still produced with processes using phosgene. From literature a method of PC production using BPA and diphenyl carbonate by transesterification in the melt is found and the general reaction conditions are explained (Braun et al., 2012). This reaction does not require the use of phosgene. Note that the experimental procedure is performed on laboratory scale.

A 250 ml three-necked flask is fitted with a metal stirrer, nitrogen inlet, a 30 cm Vigreux column and a condenser for distillation with a vacuum adapter and a receiver flask. 9.12 g (0.04 mol) BPA and 9.42 g (0.044 mol) diphenyl carbonate are combined with 1.6 mg sodium methoxide and placed in the reaction flask under a stream of nitrogen. Pressure is then reduced to 30 Torr and the flask is placed in a preheated metal bath of 150° C, during which the components melt. The mixture is stirred and gradually heated to 220° C (1° C/min). When the larger part of the phenol is distilled off, the pressure is reduced to 7 Torr and the mixture is heated to 235° C for 1 h. Then the mixture is heated to max 300° C for another 2 h. The mixture is kept under these conditions until the mixture becomes very viscous. Now the vacuum is released and the molten mixture is poured into a porcelain dish.

Poly(methyl methacrylate) (PMMA)

PMMA is the most commonly found waveguide material. It is fabricated from the monomer methyl methacrylate which is a liquid at room temperature and polymerization starts when a free radical initiator is added to the solution. When the mixture is heated the radical initiator decomposes and the free radicals cause the polymerization process. Free radical initiators often used are benzoyl peroxide (BPO) or azubisisobutyronitrile (AIBN). The chemical structure of both the monomer and polymer of methyl methacrylate can be seen in Figure 4.1.

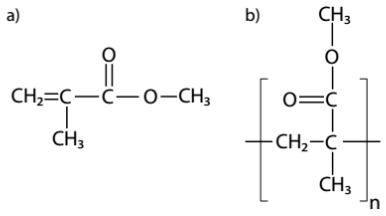

Figure 4.1: Methyl methacrylate (a) and PMMA (b) (Wilson, 2010).

A detailed description of the polymerisation process is explained in literature (Wilson, 2010). This process requires monomer, polymer and an initiator (AIBN). First, monomer and polymer are weighed in the ratio of 9:1. Lu-

minophores used in the LSC are at this step dissolved in the monomer. Next, the monomer is heated to 60° C under stirring and the polymer powder is added while stirring. This mixture is stirred for 1 hour. After the polymer powder has dissolved the mixture is removed from the heating source and allowed to cool at room temperature. 0.08% by weight of AIBN is dissolved with a small amount of pure monomer and is then added to the mixture and this is stirred thoroughly to disperse the initiator throughout the mixture. This mixture is then ready to be poured into the LSC mould.

P(LMA-co-EGDM)

This waveguide material is used in the LSC that use QDs as luminophores. Similar to PMMA, the luminophores are dissolved in the monomer mixture prior to the polymerisation process. The reaction process is explained in literature (Bomm et al., 2011). First the QDs are dispersed in a monomer mixture of lauryl methacrylate (LMA) together with 20 wt% of ethylene glycol dimethacrylate (EGDM) and 0.1 to 0.5 wt% of the liquid UV-initiator Darocure . Mixing is done by ultrasonic treatment. After mixing the reaction mixture is transported to the glass cuvettes and polymerisation takes place during the illumination from two sides with UV-A radiation of 360 nm for 15 minutes. After this initial step the polymerized plates were taken out of the cuvettes and illuminated for an extra 2 hours to complete the process. The chemical structure of P(LMA-co-EGDM) is shown (Figure 4.2).

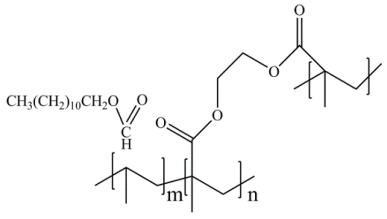

Figure 4.2: Chemical structure of P(LMA-co-EGDM) (Yuan et al, 2012).

Unsaturated polyester

Although PMMA is the most conventional waveguide material it has often negative side effects such as the deterioration of the photo-stability of the luminophores due to reaction with required additives or the presence of monomer residues (Seng Lim et al., 2012). Unsaturated polyester (UP) is a waveguide material introduced as a possible alternative. The UP is mixed with MMA to modify the chemical structure during polymerization. Preparation of the waveguide is as follows (Seng Lim et al., 2012). The required reagents are UP mixed with styrene (31.5 +/- 2% of total weight), methyl ethyl ketone peroxide (MEKP), MMA and the luminophore (Rhodamine 6G in this study). A metal

mould was used to produce the LSC sheets. First the reagents are weighted in the required proportions. As can be seen from the structure of the final LSC waveguide product (Figure 4.3) the molar ratios are:

- 2 molar of UP resin
- 3 molar of MEKP
- 1 molar of styrene
- 1 molar of MME

The amount of Rhodamine 6G can be varied. The Rhodamine 6G, UP resin and MMA are mixed and stirred until the Rhodamine 6G is evenly dispersed. Then the catalyst, MEKP is added to initiate the polymerisation process and kept aside for 20 minutes for natural degasification. The inner sides of the metal mould are treated with wax and poly(vinyl alcohol) solutions as a release agent. Then the mixture is added to the mould and is allowed to harden for 4 hours. After the mould is removed the sheet is placed in the oven to cure at 50° C for 14 hours and at 75° C for 3 hours to complete the process.

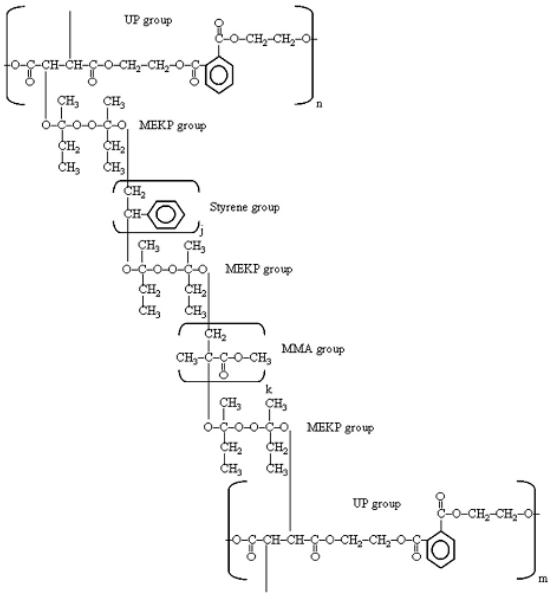

Figure 4.3: Chemical structure of the unsaturated polyester (Seng Lim et al., 2012).

Polylactic acid

Polylactic acid (PLA) is a carbohydrate that can be produced from starch and sugars and can be biodegraded to CO_2 and H_2O therefore it is a more sustainable

chemical compared to the readily available and commonly used PMMA (Fattori et al., 2011). The physical properties are in the same range as PMMA thus making PLA an interesting substitute. The synthesis process used in the study is as follows. LL-lactide (2.12 g) was heated in a Schlenk tube in the presence of the initiator $Sn(Oct)_2$ (0.5 mol%) at 130° C for 3 hours. Around 1 wt% of luminophore was used in the reaction process to incorporate the luminophores in the PLA product. After reaction the purification step consisted of dissolution of the crude polymer in chloroform and the slow precipitation by n-hexane. The then purified polymers were separated by a Büchner funnel and dried overnight in vacuum at room temperature. The chemical structures of the reactants and polymers used are shown (Figure 4.4).

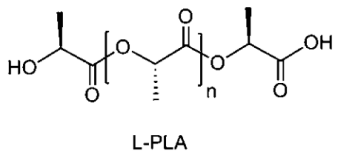

Figure 4.4: Chemical structure of PLA (Fattori et al., 2011).

Polyvinyl-butytal film

In a study conducted by Saraidarov luminophores have been incorporated into polyvinyl-butyral (PVB) films. The PVB films used were 80% PVB and had polyvinyl-alcohol and polyvinyl-acetate incorporated as can be seen in Figure 4.5. The luminophore used was DH-$BP(OH)_2$ (Saraidarov et al., 2010). The synthesis procedure as found in the paper describes the following steps. First, 0.01 g of the luminophore was dissolved in 1 ml of $CHCl_3$ and added to 5% PVB in 20 ml of chloroform solution. Then, 10 ml of ethanol, 3 ml of dimetyl-formamide and 10 ml of propanol were added to obtain transparent polymer solution. Then to 10 ml of this solution 1 ml of ethanol was added and films were obtained by dip-coating technique and heated at 80° C for 15 min.

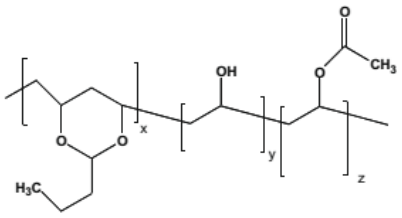

Figure 4.5: Chemical structure of PVB (Saraidarov et al., 2010).

The preparation of PVB is explained in literature (Braun et al., 2012). For

this process 3.3 g of distilled butanal (butyraldehyde) is placed in a 250 ml three-necked flask which is fitted with a stirrer, reflux condenser, and dropping funnel. The poly(vinyl alcohol) (5 g) added to 50 ml of water that has been warmed to 65° C and to which 0.3 g of concentrated sulphuric acid has been added. This mixture is slowly dropped into the flask under continuous stirring. The addition should take around 2 minutes. The polymer precipitates immediately. now 1 g of 50% sulphuric acid is added and the mixture is allowed to react at 50°-55° C for another hour. After cooling to room temperature the mixture is filtered and washed with water until it is neutral. Then it is reprecipitated from methanol solution into water, filtered and dried under vacuum at 40° C. A film can be created by spreading the solution on a glass plate and allowing for evaporation.

4.2.2 Luminophores

For this LCA study two types of luminophores are considered. Organic luminophores and QDs. These are produced separately from the waveguide material and during the production process incorporated into the waveguide prior to the casting process to end up with the LSC sheet. The selection of luminophores is based on a literature study which reported the efficiencies of the produced LSCs in combination with an attached photovoltaic cell. These luminophores are:

- Lumogen F Red 305 from BASF company.
- Perylene Perinone.
- CRS 040 from Radiant Color
- CdSe/CdS/$Cd_{0.5}Zn_{0.5}S$/ZnS

The different syntheses methods, if available, to produce the luminophores are described below. Often only a small amount of luminophores is dissolved in the waveguide since a high concentration increases the chance of reabsorption of emitted radiation by other luminophores.

Lumogen F Red 305

This luminophore is produced and sold by BASF chemical company. It is a substituted perylimide produced by a patented process (Seybold et al., 1989). The synthesis methods are not directly available but it is likely to consist of a multistep process in which different sidechains are systematically added. The chemical structure (Figure 4.6) shows the complex nature of the molecule (Wilson et al., 2010).

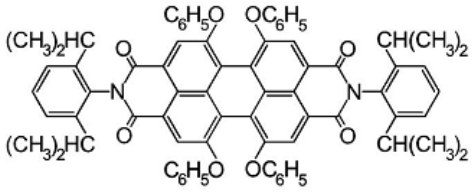

Figure 4.6: Chemical structure of Lumogen F Red 305 (Wilson et al., 2010).

Perylene Perinone

The compound used in combination with Lumogen F Red 305 for the production of a 4.2% efficient LSC (Desmet et al., 2012) has had other applications in the past but has now been used to act as a luminophore. The compound is synthesised in a two-step reaction process (Debije et al., 2011). The first reaction step starts with 1,6,7,12-tetrachloroperylene-3,4,9,10=tetradicarboxydianhydride (TCP TDC) (3.8 mmol) and o-phenylenediamine (17.1 mmol) to which 30 ml propionic acid was added. This mixture was then stirred at 140° C for 6 hours, cooled to around 85° C and filtered. This product was then washed with 15 ml of warm propionic acid followed by a large amount of water after which it was dried at 80° C for 10 hours. The reaction yield was 62%.

For the second step 3 g (4.4 mmol) of the previous product, nonyl phenol (26.4 mmol) and potassium carbonate (26.4 mmol) were added to 60 ml of N-methylpyrrolidone. This mixture was then stirred at 140° C for 24 hours and cooled to room temperature. It is then treated with 10 ml of cold concentrated HCl in an ice bath until gasses stopped producing. The precipitate was then filtered and washed repeatedly with water, and then 5 times with 30 ml of methanol. The final product was purified using a silica gel HPLC using a 40%-70% dichloromethane-hexane mixture. The structure of the final product (Figure 4.7) shows both the anti and syn orientation of the product with R being the nonyl functional group.

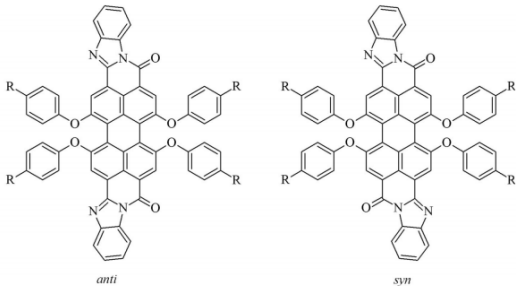

Figure 4.7: Chemical structure of Perylene Perinone (Debije et al., 2011).

CRS 040

This is an organic luminophore obtained from Radiant Colour company. It is a coumarine which can also be combined with Lumogen F Red 305 to produce a LSC. Little is available on the chemical characteristics of this compound.

CdSe/CdS/$Cd_{0.5}Zn_{0.5}$S/ZnS

These type of multi-layered QDs have their CdSe core protected from the surrounding by adjacent layers of material. This increases their photostability. Also a synthesis method (SILAR) has been developed (Xie et al., 2004) to gradually change the layer composition to have both the structural benefits from the CdS and the electronic benefits from the ZnS synthesis of these QDs. The process consists of three steps. First the CdSe core QDs have to be synthesized. To do this, a mixture of 0.0514 g of CdO powder, 0.224 g of tetradecylphosphonic acid (TDPA), and 4 g of tributylphosphine oxide (TOPO) was mixed for 1h at 320° C under argon flow. The temperature was then lowered to 270° C after which a solution of 0.0632 g of Se in 2 g of tributylphosphine (TBP) was injected.

Then the temperature was altered to 250° C for 1 minute. Then the heat source was removed and 15 mL of methanol was injected at 100° C causing the precipitation of the QDs. Finally the particles were dispersed in chloroform or toluene for further processing.

Second the precursor solutions have to be synthesized which contained CdO, ZnO, elemental sulphur, and selenium. For a 0.1M zinc solution, 0.2034 g of ZnO is dissolved in 6.18 g oleic acid and 18 mL 1-octadecene (ODE) at 240° C. Similar procedures were used for the Cd and Zn/Cd solution which were kept hot after the process. The sulphur solution was made by dissolving sulphur in ODE at 180° C which was then allowed to cool to room temperature.

These precursor solutions are used in the synthesis process of the QDs. For this, 3 mL of ODE and 1 g of octadecylamine (ODA) were mixed in a reaction vessel and heated to 100° C under vacuum for 1h and then cooled to room temperature. To this, 1.83 x 10^{-7} mol of CdSe QDs were added and heated to 100° C for 30 minutes under vacuum to get rid of the undesired materials. Then, the mixture was heated to 250° C under argon flow. To this mixture the different precursor solutions were added in calculated amounts in steps taking 10 minutes. When this process was finished, the mixture was allowed to cool to room temperature. Hexane (10 ml) was added and the unreacted reagents and by-products were removed by methanol extraction until the methanol was clear and the complete QDs were produced.

4.2.3 Waveguide and luminophore mixing and casting

In general the luminophores are combined with the waveguide material when the polymerisation process starts since it is easier to obtain an even distribution when the waveguide is still in the monomeric form. Depending on the type of LSC that is produced a certain weight percentage (wt%) of luminophores is

added to the waveguide mixture. These values typically range from 0.003 wt% to 0.01% in the experimental studies performed (Desmet et al., 2012; Slooff et al., 2008; Bomm et al., 2011). Then, the polymerisation process starts under the required conditions described earlier. During/after this stage, the mixture is drop casted or injection moulded into the LSC mould. After the polymerisation process has finished, the mould is removed and the LSC sheets are obtained. Sometimes post-curing is required if not all the monomers have reacted since an excessive percentage of monomers affects the photostability (Wilson et al., 2011) and a percentage of 0.5% is accepted by industry. This can be achieved by heating the sheet above the glass transition temperature in a hot-air oven. After the curing of the slabs is finished, cutting into the required square or rectangle shape is done and protective measures such as tape is applied to prevent the LSC sheet from scratching. The sides are allowed to remain rough since this allows the PV cells to better bond with the sheet during the assembling.

4.2.4 Photovoltaic cells and assembling of sheets with cells

When the LSC sheets are fabricated a PV cell is glued to one or multiple sides of the sheet to convert the concentrated light beam into an electric current. For this different types of PV cells can be used to achieve different types of conversion efficiencies. The most commonly used cells to date are based on silicon due to the abundancy of the material and the economic price. Either monocrystalline silicon (mc-Si) or polycrystalline silicon (pc-Si) is used and attached. Another used PV cell is the GaAs cell which has higher conversion efficiencies but is also more expensive due to the materials used. This section aims to describe the different industrial processes required to produce the PV cells which are assembled with the LSC sheet and explaining the process of attaching the cell to the sheet.

General silicon production

For both mc-Si and pc-Si the same starting ingredient, solar grade silicon, is required. The process starts with the production of silicon from quartz sand mixed with a source of carbon (e.g. woodchips or charcoal) and is heated in an electrical arc furnace to form silicon and CO. Raw materials are selected to achieve high product quality, to achieve high performances and minimise the environmental damages. The reactivity and consistency of the materials are important factors which affect the furnace performance in terms of yield, power consumption and product quality (Ceccaroli et al., 2011). The overall reaction and individual reaction steps are (Ceccaroli et al., 2011):

$$Overall : SiO_2(s) + 2C(s) \rightarrow Si(l) + 2CO(g) \tag{4.2}$$

$$Si(l) + \frac{1}{2}O_2 \rightarrow SiO(g) \tag{4.3}$$

$$SiO(g) + \frac{1}{2}O_2 \rightarrow SiO_2(g) \tag{4.4}$$

Reaction 3 and 4 occur when an open furnace is used. The silica fumes are then released in the atmosphere. Depending on the conditions 10 to 20% of the silica can escape in the form of these fumes. Filters are applied to retrieve the silicon and these particles find application as additives in concrete and refractory. Reactions 1, 2 and 3 explain the simplified processes occurring in the furnace. Two important intermediate compounds are gaseous silicon monoxide (SiO (g)) and solid silicon carbide (SiC (s)). To illustrate the more complex processes occurring in the furnace a distinction can be made between reactions occurring in the inner hotter zone (range of 1900°2100° C) and the outer cooler zone (lower than 1900° C).

$$2SiO_2(l) + SiC(s) \rightarrow 3SiO(g)_+CO(g) \tag{4.5}$$

$$SiO(g) + SiC(s) \rightarrow 2Si(l) + CO(g) \tag{4.6}$$

$$SiO(g) + 2C(s) \rightarrow SiC(s) + CO(g) \tag{4.7}$$

$$2SiO(g) \rightarrow Si(l) + SiO_2(g) \tag{4.8}$$

Due to the high temperature required for the reaction small batches of reactants are continuously added to the furnace and liquid silicon is drained out from the bottom. This silicon still contains 1 to 4% of impurities depending on the materials and electrodes used (Ceccaroli et al., 2011). This product is called metallurgical-grade silicon.

Solar grade is another commercial grade of silicon with a higher purity compared to metallurgical-grade silicon. This is mostly produced by the Siemens process where trichlorosilane ($SiHCl_3$) is thermally decomposed on a heated silicon rod inside a deposition champer. The $SiHCl_3$ is prepared by hydrochlorination of metallurgical-grade silicon (Ceccaroli et al., 2011). Trichlorosilane ($HSiCl_3$) is prepared by hydrochlorination of metallurgical grade silicon in a fluidised bed reactor. As a side product tetrachlorosilane is formed in a molar proportion of 10 to 20%. Both reactions are given:

$$Si(s) + 3HCl \rightarrow HSiCl_3 + H_2 \tag{4.9}$$

$$Si(s) + 4HCl \rightarrow SiCl_4 + 2H_2 \tag{4.10}$$

As $HSiCl_3$ has a low boiling point of 31.8° C it undergoes two purification steps, one to decrease the level of boron and phosphorus down to the ppb levels and a second step to eliminate the components lighter than $HSiCl_3$. Next the compound is diluted with hydrogen and led into the deposition reactors containing the heated silicon seed rods. These rods are electrically heated to 1100° C on which hyper pure silicon will grow. By products leaving the reaction during and after this process are H_2, HCl, $HSiCl_3$, $SiCl_4$ and H_2SiCl_2. The main reactions occurring in the chamber are:

$$2SiHCl_3 \rightarrow SiH_2Cl_2 + SiCl_4 \tag{4.11}$$

$$SiH_2Cl_2 \rightarrow Si + 2HCL \tag{4.12}$$

$$H_2 + HSiCl_3 \rightarrow Si + 3HCl \tag{4.13}$$

$$HCl + HSiCl_3 \leftrightarrow SiCl_4 + H_2 \tag{4.14}$$

Earlier the fumed silica produced during the production of metallurgical-grade silicon could be used during the production of hyper pure silicon as it reacted with the $SiCl_4$ to produce high quality silica but due to the growth of the industry other approaches had to be adopted. Often closed-loop production processes are used to recycle the $SiCl_4$ that is formed to increase the productivity of the plant and reduce the environmental and economic burden. Other processes are known to produce high grade silicon but the Siemens process accounted for at least 60% of the production in 2001 (Ceccaroli et al., 2011). In 2008 this share was as high as 78% (Xakalashe et al., 2011) but expectations are that this share will go down again in the near future due to competition from other technologies (ITRPV, 2013). The solar grade silicon that is now available is used as a feedstock material for both the production of monocrystalline and polycrystalline silicon. A graphical illustration of the processes from quartz sands to photovoltaic cells is illustrated (Figure 4.8).

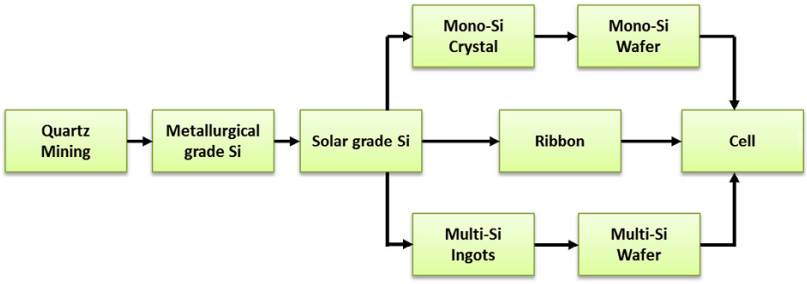

Figure 4.8: Illustration of production pathways from quartz to final PV cell assembly (Yue et al., 2014).

Monocrystalline silicon

The solar grade silicon (SoG-Si) produced by the Siemens process is further processed to form a mc-Si wafer. First the SoG-Si is grown to crystals using the Czochralski process. In this process the feedstock is molten in a crucible and a seed crystal of high crystallinity is dipped into the molten silicon and slowly pulled out of the melt allowing the liquid to crystallize at the seed. This is called crystal pulling and results in a highly crystalline cone on the crystal seed. The length of the cone commonly is between 200 and 400 cm.

Polycrystalline silicon

Poly (or multi) crystalline silicone is mostly produced using the Bridgeman technology which requires a single crucible. The other method, called the block-casting technique, requires two crucibles and was used by two companies in 2008

(Rodriguez et al., 2011). In the Bridgeman process, silicon is molten in a Si_3N_4 coated quartz crucible (Figure 4.9). The silicon is crystalized by lowering the crucible out of the heated zone or by raising the heated zone out of the crucible. In this way silicon ingots of 450 kg (90 x 90 x 30 cm) have been successfully realised.

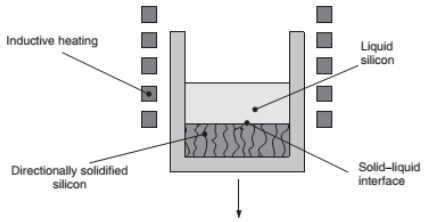

Figure 4.9: Illustration showing the Bridgeman process where the crucible is positioned between the heating elements and solidified silicon is forming at the bottom of the crucible (Rodriquez et al., 2011).

Wafering

Most of the wafering is done by wire cutting of pre-cut silicon ingots of the size that is desired (typically 15 x 15 cm) by a multi-wire sawing technique. In this process a single wire (stainless steel) passes four rollers allowing it to pass the column parallel over 1000 times and the wire is pulled through the silicon column to cut wafers of pre-determined sizes. This process is similar for both mono- and polycrystalline silicon. A slurry of polyethylene glycol (PEG) and SiC granules is used to both slice through the silicon column and to prevent the agglomeration of the wafers. The wire used can have lengths of over 500 km and a common cutting speed of 0.3 mm / min can be maintained. After the cutting process the surfaces of the wafers are damaged and contaminated from the slurry used so it needs to be (chemically) etched.

Cell manufacturing

The wafers that are produced during the previous explained step need to be processed through various steps to make them suitable for photovoltaic applications. During several processes the surface of the wafers is altered and several layers are added in order to achieve a module that has electrical properties required for the application that is desired for the module. Each of these steps are briefly explained. An illustration showing how the different steps alter the wafer is given (Figure 4.10). The process starts with wafers originally round in shape but which are very often trimmed to be either square or pseudo-square (squares with cut-off corners) with typical side dimensions of 12.5 15.6 cm.

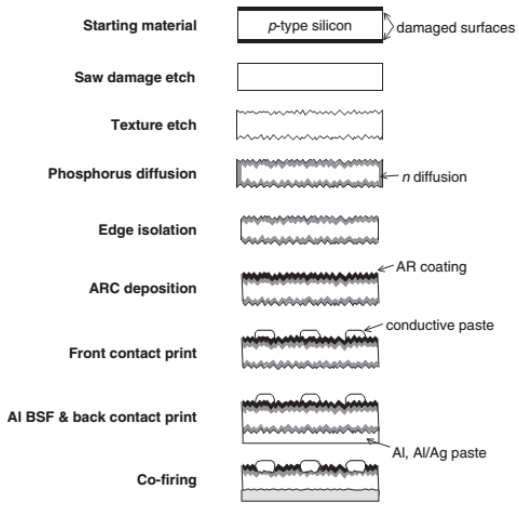

Figure 4.10: Scheme showing the different steps required in the cell manufacturing process (Tobis et al., 2011).

1. Saw damage removal: After the cutting process the surfaces are left with a high degree of damage. This reduces the quality and increases the chance of breaking. In this step, about 10 μm is etched off each side in alkaline or acidic solutions. Another option is to use plasma etching.

2. Texturization: In order to achieve good performance an uniform pyramid like surface needs to be realized on the wafer. Their size is important since small pyramids lead to high reflection while large pyramids hinder the formation of the contacts. Several processes can be used in the texturization process. Acidic texturing can in some cases be performed simultaneously with the saw damage removal process. Plasma texturing uses reactive ions and can be performed under dry conditions, however has the downside of the high global warming potential of the used chemicals. Mechanical texturing can be achieved by using a conventional dicing saw and bevelled blades followed by alkaline etching to decrease the surface damage

3. Phosphorus diffusion: Phosphorus is the universal applied n-type dopant for silicon in solar cells. Due to the high temperature conditions it is important that the surfaces are free of impurities, therefore an acidic washing step is used prior to the diffusion step. Two methods exist for applying the dopant layer. Quartz furnaces are tubes in which the cells enter and leave on one side of the furnace. Gasses enter the furnace from the other side. Phosphorus can be supplied by bubbling N_2 gases through liquid $POCl_3$. It is also possible to use solid dopant source. A representative procedure takes 20 30 minutes at 830 860° C. The other option is to use

belt furnaces. In this procedure the dopant is first applied on top of the wafers through various processes (e.g. screen-printed, spun-on). Infrared heating allows for fast heating and cooling and similar temperature profiles as found in the quartz furnace procedure are applied. The downside of the belt furnace is that air can flow through and this can be a source of metallic impurities. After the diffusion steps a layer of phosphosilicates remains at the surface that is often etched off in dilute HF because it can hinder the later processing steps.

4. Edge isolation: After the application the n-type region can be all over the wafer. At the rear it forms no problem since it will be compensated by the excessive aluminium that is applied later. However the edges need to be free since this would provide a shortcut for the back and front contacts that are applied later. This lower resistance path would shunt the front and backsides and should therefore be removed. Several procedures can be used to remove this region. The most widely used procedure is laser grooving. Another option is to again use chemical etching.

5. ARC deposition: The antireflection coating (ARC) was traditionally from TiO_2 but nowadays hydrogenated silicon nitride films are preferred as it combines several properties. Application is preferably done by chemical vapour deposition (CVD) making use of the reaction of silane gas and ammonia. Plasma-enhanced CVD is the preferred option because it is a low-temperature process ($< 500°$ C) which is less complicated and prevents lifetime degradation. Several systems to apply the ARC exist, e.g. direct-plasma reactor and remote-plasma system.

6. Front contact print: Due to the various requirements for the front contacts silver is the preferred metal. Copper is a second but due to the repetitive heating steps required its high diffusivity will contaminate the wafer. Although screen printing is not the perfect technique to apply the front contacts (vacuum evaporation is preferred) the high throughput and associated costs compensate for this. The silver paste is a viscous liquid and after application the solvents are evaporated in an in-line furnace at 200 250° C.

7. Al BSF and back contact print: The p-type region at the back of the wafers is formed by screen-printing an aluminium paste, making up the back-surface field (BSF) layer. During this process, some silicon will dissolve in the Al. Since the soldering of contacts is not possible, busbars are printed which will form the arrays of the cells in the module.

8. Co-firing: After the previous explained process the different metallic compounds require a heating step to improve connection, while simultaneously burning of the excessive organic compounds from the paste. This is a very temperature dependent process as too high temperature will result in short circuiting the cell, while too low temperatures will be not sufficient. Also, the thermal properties of the Al-paste are different compared to the silicon

resulting in slight bending of the cells which can be prevented by rapid cooling after the co-firing step.

Once these steps are finished the photovoltaic cells are tested and sorted according to their output. Multiple cells with similar outputs are then combined to produce a module. For this tinned copper ribbons (tabs) are used to connect the front of one cell to the rear of the adjacent one. This way 9 to 12 series-connected cells are formed. Complete modules typically consist of 72 cells of 125 x 125 cm^2 or 60 cells of 156 x 156 cm^2. The cells have to be protected from weathering, humidity, be resistance to impact and electrical insulated. For this the inter-connected cells are laminated in a sandwich of several layers, starting with a glass pane on top, two polymer sheets above and under the cells, and a back layer. As a polymer, ethylene vinyl acetate (EVA) is the most used. No in depth overview of the techniques for module fabrication is provided as this is beyond the scope of LSC modules, in which cells are attached and insulated in a different way.

GaAs

A more efficient solar cell compared to the previously described silicon modules are solar cells using a combination of gallium and arsenide. Currently these are not widely produced due to the high costs of the modules which is currently not compatible with the cheaper available solutions. However when combined with LSC the small size required and the increased output due to the concentrated beam hitting the surface of the GaAs cell it might result in a cost wise more favourable combination.

GaAs cells are less commonly applied and little is known about the specific production conditions since this if often propriety and confidential information of the various companies involved in the photovoltaic production. However it is possible to get a general idea of the processes and materials involved. GaAs cells are produced on large sized GaAs wafers by a low-pressure metal organic chemical vapour deposition (MOCVD). Originally this process was very expensive since the wafer could not be used multiple times in a row since the removal step would alter the surface of the wafer. However using the epitaxial lift-off (ELO) process theoretically offers the possibility of re-use (Bauhuis et al., 2009). In this process the thin-film cell structure is separated from the substrate by the wet chemical etching of an intermediate sacrifice layer (AlAs). This sacrifice layer thus allows the wafer to be used multiple times before MOCVD becomes impossible. By growing the cell structure in reverse order it is possible to incorporate all the required junctions as well as the mirror layer. Two sources describing the methods and materials are summarized below.

Using MOCVD at a temperature of 700° C and a pressure of 20 mbar a GaAs cell with a carrier concentration of 6.5 x 10^{-18} cm was formed (Bauhuis et al., 2009). In this process arsine and phosphine were used as group-V source gasses and trimethyl-gallium, trimethyl-indium and trimethyl-aluminium as group-III precursors. For doping disilane and dimethyl-zinc were used. A release layer of

AlAs with a thickness of 10 nm was grown before the layer structure. The layer structures had an AlInP window and an $(Al_{0.4}Ga_{0.6})_{0.52}InP$ back surface layer and a base layer thickness of 2 μm. Then the lift-off process is performed (wet chemical etching in HF) after which the backside of the cell is open to air. It is on this side that the p-type metal contact is deposited by e-beam evaporation, after which the thin film is glued to a glass carrier and the support is removed. On the backside Au contacts were used and on the frontside Pd/Ge/Au was applied using e-beam evaporation. Then the contacts were electroplated with Au to a thickness of 5 μm. Finally a ZnS/MgF_2 anti-reflection coating was deposited by e-beam evaporation.

Another similar procedure has been applied on industrial scale (Youtsey et al., 2012). MOCVD at 100 mbar was used to grow the structures. The chemicals used were AsH_3, PH_3, trimethyl-indium, trimethyl-gallium as precursors using a V/III ratio of >50. Inverted metamorphic multijunction InGap/GaAs/InGaAs structures were grown on GaAs substrates. The first layer deposited is a thin AlAs release layer (5 nm). Then the solar cell layers are deposited followed by a thick flexible metal carrier layer. Here the same wet chemical etching procedure is used using HF to remove the AlAs layer. The AlAs layer has a higher etch selectivity relative to the GaAs structure ($1x10^5$), meaning that there is almost zero etching damage on the GaAs layer. Next, the solar cell device is further processed (Ti-Au grid metallization, wet etch isolation, TiO_2-Al_2O_3 antireflection coating, device singulation). Last, the completed solar cells are removed from the temporary carrier. The wet chemical etching process is illustrated (Figure 4.11). By this process cells as large as 20 cm^2 have been fabricated, which is small compared to silicon cells which can be ten times larger. However possible applications of these cells are in potential different fields such as LSCs, as mentioned before.

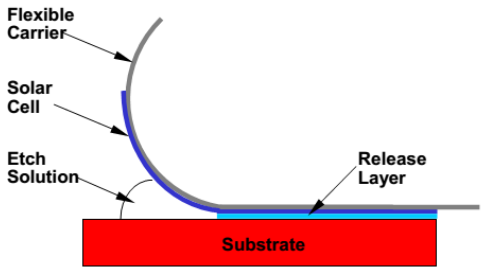

Figure 4.11: Schematic depiction of the wet chemical etching of GaAs thin-films (Youtset et al., 2012).

Assembling of PV with LSC sheet

After the cutting process of the waveguide slab containing the luminophores into the desired shape the edges are rough from the sawblade. This helps the

attachment of the PV cells with the LSC sheet. A two-part epoxy resin can be used (Wilson et al., 2012) which firmly attaches both components. Since this glue is transparent and has similar optical properties compared to the waveguide almost no losses will occur when the light moves through this small layer. However it is important to avoid any glue around the top or bottom side of the sheet since due to the light scattering in the waveguide any light that is absorbed by excessive glue near the edge of the sheet is escaped and cannot be retrieved. This can be avoided by applying a small mirror on both sides of the LSC preventing any glue from touching these surfaces. Both the situation with and without mirrors are illustrated (Figure 4.12). After the attachment of the photovoltaic cells to the waveguide the LSC is nearly complete. Some of the extra components found in literature are shortly discussed and the next section will explain the BOS components that are required to be able to use the LSCs combined in a framework as a BIPV module.

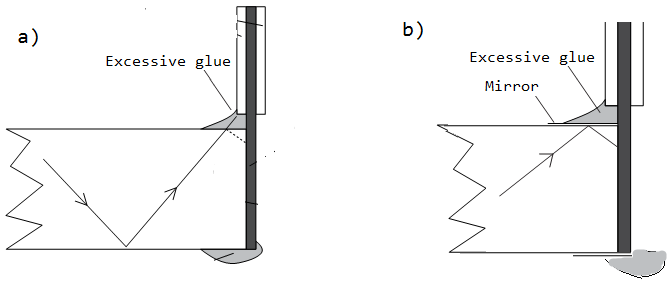

Figure 4.12: Illustration showing the inner waveguide reflections with (a) and without (b) a mirror applied. Illustration was retrieved and altered Wilson (Wilson et al., 2012).

4.2.5 Other materials used

The previous paragraphs already described the largest share of materials that are required to produce a LSC module. However in the literature that is used as a reference for the different combinations of materials that make up one LSC module several other components are mentioned that fit not in one of the categories, therefore they are mentioned here. Not all modules use the all of these components, however most of the ones mentioned below are generic and are applied on all modules as they serve a role in either protecting the cell from outside conditions or serve to increase the yield from the cell.

MCPET back-reflector

A microcellular foamed reflector (MCPET) has been developed by Furukawa, a Japanese electric company. It is a foam produced from poly(ethylene terephthalate) (PET). The original idea to produce microcellular foamed plastic was

developed at MIT in the 1980s to save material and weight (Han et al., 2013). The technology generates cells whose sizes are 10 μm or less in densities of 10^9 cells/cm^3. A gas is used as a blowing agent expanding the plastic. Due to the low quantities used and the product being commercial available an in depth production pathway is not provided, however the production process of a similar MCPET look-a-like is explained (Han et al., 2013). First, the gas is mixed with PET under high pressure. Then the mixture is transferred to atmospheric pressure and the temperature is increased. Due to the low solubility of gas under these conditions the gas is eluted and the cells are formed. Currently the MCPET back-reflector finds it applications in the lighting sector to enhance the luminescence from e.g. LED lights. If combined with LSCs it can decrease the amount of light escaping from the backside of the waveguide material.

Aluminium mirrors

Regarding the aluminium mirrors that are applied to increase the performance adhesive 3M visible mirror foil with 97% reflection can be purchased from 3M (Sloof et al., 2008). These are tapes having an aluminium layer implemented that reflects both heat and light.

Diffuse reflector

The same authors that apply aluminium mirrors to their LSC units also choose to use a diffuse reflector at the rear side of the module. The principle of a diffuse reflector is that it scatters the incoming rays at many angles. This could also increase the performance of the LSC module, as it scatters light that could be lost back to the module. It is unclear from the literature if the reflector is placed under the module or if the reflector is attached directly on the module.

Low-iron soda-lime glass

In order to prevent scratching, and protect the cells from both humidity and wind effects a 6 mm thick low-iron soda-lime glass is placed as a front cover. Low-iron glass has the benefit that it has a low absorption thus it can achieve the highest light transmission towards the LSC sheet (Wilson, 2010). This glass layer has to be separated from the LSC sheet by a small air gap to prevent light to be trapped in the front cover. A similar glass is placed at the rear of the module for the same protection reasons. However as this does not require a high optical transparency this can be made of regular soda-lime glass. This layer is often 4 mm thick. A visualisation of the glass layers combined with the LSC sheet is provided (Figure 4.13).

Tabbing

For the current to flow from the cells through a wire tabbing has to be applied. In the case of LSC cells the PV that has to be connected is very small in area, smaller than conventional PV, therefore the amount of tabbing required is also

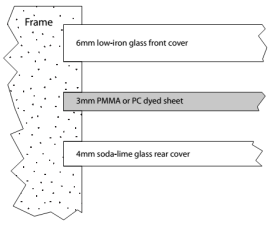

Figure 4.13: A schematic illustration of how the two glass layers and the LSC sheet are combined with the aluminium framework to build up a module (Wilson, 2010).

very small. Tabbing consists of small copper wires that are soldered on the front side of one cell and are connected to the rear side of the adjacent cell. As the cells that are attached to the LSC sheets are smaller than common cells which require multiple tabs, based on literature it is assumed that for each cell, two tabbings are installed (Wilson, 2010). In the case of a 3 mm thick LSC sheet this would have a dimension of 2 x 0.25 mm.

Aluminium frame and wiring

In order to have a fixed framework around the different cells that make up the module an aluminium frame is built around the cells to provide rigidity and ease the instalment of the BIPV modules. This framework would resemble a raster with thicker dimensions on the sides than on the inner part, since most stress would be assumed on the outer sides of the module. This is also called an aluminium curtain walling framing that is widely applied in modern architecture for constructing large glass walls that are used in e.g. office buildings. A module resembling this structure has been built in the past (Aste et al., 2015) and an illustration is provided (Figure 4.14). Wiring that connects the several cells that make up the module can be applied and incorporated in the aluminium frame so that each frame has only one output cable. An assumption of the amount of aluminium that is required could be calculated by looking at the LSC cell size and the number of cells that make up for example 1 m^2 of module.

Attachment of BOS components

Now that the LSC module is fabricated BOS components need to be added in order to get the power produced by the cells transported to where it is needed. Several components are required in order to use this electricity in household appliances or to feed the excess energy to the grid. In most cases the share of environmental impacts from the BOS components is smaller than the photovoltaic modules, however as the environmental impacts for photovoltaic production decrease these values start to become significant (De Wild-Scholten et al., 2006). There is a high similarity in the products required for the BOS system

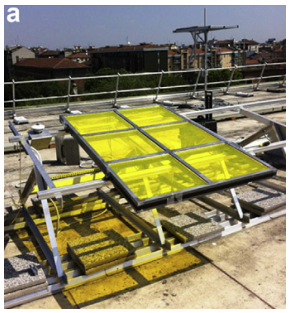

Figure 4.14: LSC module made up of sheets and framing placed on roof (Aste et al., 2015).

of conventional photovoltaics since the cells that produce the actual electricity are the same, therefore it is assumed that the same distinction between classes of materials can be made. However as an LSC module will produce a smaller current compared to conventional silicon PV based modules adjustments in the BOS components selection have to be made to account for this smaller capacity. In this section the components are listed and the production pathways to manufacture these components is discussed. It is assumed that the modules are installed on-grid, thus that current can be directed directly towards the grid. An illustration (Figure 4.15) of how the module is connected to the grid is found in literature (Whitaker et al., 2011).

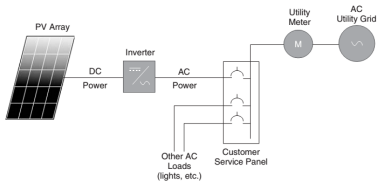

Figure 4.15: Simplified illustration showing a module connected on-grid (Whitaker et al., 2011).

Thus, in order to transport the current from the module towards the grid three extra components are required. First there is the cabling from the module towards the inverter and the cabling from the inverter to the grid. From the module towards the inverter DC cabling is used and from the inverter to the grid AC cabling is used. The other component required is the inverter. The capacity of the inverter has to match the power that is provided by the module (or multiple modules) in order to have the best conversion. Also the AC power has to match the utility grid that it is connected with. This includes the voltage and the frequency (Schmidt et al., 2011).

Array layout and inverter

First a general estimation of the area that is covered by the modules has to be made. The module that was fabricated in the paper by Atse et al. had an area of 1.75 m^2. In order to rate the module often the peak AC or DC power is used for comparison. If one compares DC power, W_P or kW_P is used to express the peak power and in case of AC power, W_{AC} or kW_{AC} is used. However these terms do not require any field measurements, they are simply derived from the manufacturer of the modules. In the case of the inverter and the associated AC power it is assumed that enough modules are attached to the inverter to meet these demands. The AC power is often assumed to be lower than the DC powers connected due to several losses such as wire resistance and heating affects. An appropriate level of over-sizing is 10 to 30% larger than the AC ratings due to these unpredictable loses. Both AC and DC peak power ratings are imprecise terms, best used to get a general understanding of the system that is installed (Schmidt et al., 2011). Efforts to establish a universal more realistic definition of the peak powers are being developed, however this is beyond the scope of this research therefore the simple AC and DC peak power definitions are used.

Thus the sum of DC peak power provided should closely match the inverter. In the case of the 1.75 m^2 module the maximum power was 14.08 W, the maximum voltage was 24.29 V and the maximum current was 0.58 A. The electrical efficiency of this module was 1.26%. The problem with LSC modules is the low peak power that is produced by the cells and the high capacity of the inverters that are used in conventional BIPV systems. A mismatch between the DC current and the inverter capacity might result in increased losses therefore a lower capacity inverter is desired. The electrical efficiencies of the LSC cells under study in this research range from 4 to 10%. If similar conditions are assumed as the study by Aste et al. the maximum power would range from 28.08 W to 105.6 W. Commercially available inverters with a capacity as low as 215 W are available and would therefore provide a good solution to be combined with BIPV modules. Due to the complexity of the manufacturing of the inverter the material and electricity used will be derived from literature (De WildScholten et al., 2006). A material overview is provided in Table 4.1. Note that this is for a 500 W inverter and the data is from 2006 so there might be an overestimation of the materials that is required.

Mounting system

Apart from the aluminium frame that holds the cells to form the module other components are required for mounting the module to the building in order to have a BIPV module. These could be bolts or screws, metal plates, clamps, hooks or other components. In the case of BIPV it is assumed that these are lower in material intensity compared to roof-mounted PV modules as the building often provides part of the framework that otherwise has to be constructed from scratch.

Table 4.1: Overview of materials and components that make up a Philips 500 W inverter (De Wild Scholten et al., 2006).

Material for inverter	*Philips PSI 500 (500 W) (g)*
Steel	78
Aluminium	682
Copper	2
Polycarbonate	68
ABS	148
Other plastics	5.4
Printed circuit board	100
Connector	50
Transformers, wire wound	310
Coils	74
Transistor diode	10
Capacitor, film	72
Capacitor, electrolytic	54
Other electric components	20

Cabling and connectors

For the cabling and connectors, the current from the module has to be transported toward the inverter through DC cabling and from the inverter to the grid through AC cabling. In the study by De Wild Scholten et al. a reference area of 44 m^2 was assumed to contain 188 meter of 4 mm^2 DC cabling and 10 meter of 6 mm^2 AC cabling. The AC cabling is assumed to be roughly the same since this is also dependent on the distance from the inverter to the grid. For the DC cabling it is assumed that per 1 m^2 of module, 4 meter of DC cabling is required. This could be lower but will most likely not be higher as 4 m is long enough to go along all the sides of the module.

4.2.6 Configuration of LSCs under study

Now that all the components have been looked into a list can be made of the different materials required for each component and the energy that is required in the different reaction steps. These components will be sorted for each LSC cells that have been reported in literature of which the electrical efficiency has been measured. Each table will encompass one cell. If similarities are present the same components will not be calculated twice.

The first step is to produce the LSC cells that will be the main components of the LSC modules. It is assumed that the sides of the frame are 2.5 cm wide and the frame measures 1 cm in between modules. In the case of 5 x 5 cm modules this would therefore result in 0.64 m^2 of cell area in a 1 m^2 module area. In the cases of larger cells this would result in 0.8281 m^2 cell area for 22.75 x 22.75 cm cells and 0.8836 m^2 cell area for 47 x 47 cm cells with 0.1719

and 0.1164 m^2 frame area respectively. The tables provided in this section show the different material inputs that are required for the module production of LSC cells having the following configurations. The inventory starts with the materials required to produce 0.64 m2 of cell area but the intensities of these materials can be multiplied to acquire intensities for the other cell areas that are assumed. From hereafter the 5 x 5 cm module is referred to as small (S), the 20.75 x 20.75 module is referred to as medium (M) and the 47 x 47 module is referred to as large (L). All cells are 1 cm thick. The following configurations are considered.

#1 Stacked Lumogen F Red 305 (115 ppm) and perylene perinone (75 ppm) dyes with a MCPET back reflector in polycarbonate and mono-crystalline silicon PV cells on two edges (5 x 5 cm) reported 4.2% (Desmet et al., 2012).

#2 PMMA dyed with 0.01 wt% Lumogen F Red 305 and 0.003 wt% CRS040 using aluminium mirrors applied to the three remaining side of the plate and a diffuse reflector at the rear side and one GaAs cel (5 x 5 cm) reported an electrical efficiency of 4.6% (Slooff et al., 2008).

#3 PMMA dyed with 0.01 wt% Lumogen F Red 305 and 0.003 wt% CRS040 and a diffuse reflector at the rear side and 4 GaAs cells (parallel on the sides (5 x 5 cm2) reported 7.1% electrical efficiency (Slooff et al., 2008).

#4 CdSe/CdS/$Cd_{0.5}Zn_{0.5}S$/ZnS QD doped in P(LMA-co-EGDM) using a single multicrystaline solar cell reported an electrical conversion efficiency of 2.8% (Bomm et al., 2011).

4.2.7 Luminophores, waveguide, and LSC cell assembly

In this section the tables are provided that contain the different reactants and processes that are the basis for the LCIA using SimaPRo software. First a table is provided that indicates the requirements to produce the luminophores and the waveguide containing cells. Then a table is provided that indicates the required materials to produce the actual cells that can generate an electric current by applying e.g. the photovoltaic cells. This process is repeated for all four cell configurations.

Table 4.2: Reactants and production steps to produce the sheets for LSC #1

Material	**Quantity**	**Source**
Reactants	Unknown	*None found*
Process energy	Unknown	
Product	Lumogen F Red 305	
	3.3536 g	
Material	**Quantity**	
TCP TDC	10.71 mmol (5.67 g)	*Debije et al., 2011*
o-phenylenediamine	48.19 mmol (5.21 g)	
Propinionic acid	126.82 ml	
Water	1409.17 ml	
Process energy	Unknown	
Product	Intermediate compound	
	6.64 mmol (62% yield)	
Intermediate compound	6.64 mmol (62% yield)	
Nonyl phenol	39.87 mmol (8.78 g)	
Potassium carbonate	39.87 mmol (5.51 g)	
N-methylpyrrolidone	90.6 ml	
Concentrated HCl	15.1 ml	
Water	755.2 ml	
Methanol	226.56 ml	
Process energy	Unknown	
Product	Perylene Perinone	
	3.0208 g	
	2.266 mmol	
Material	**Quantity**	
BPA	2754.6 g	*Braun et al., 2012*
Diphenyl carbonate	2846.7 g	
Sodium methoxide	348.16 mg	
Lumogen F Red	3.3536 g	
Perylene Perinone	3.0208 g	
Nitrogen flow	Unknown	
Process energy	Unknown	
Product	LSC sheets (256)	*Desmet et al,. 2012*
	2 x (5 x 5 x 0.5 cm) $\rightarrow$ 6400 cm^2	

Table 4.3: Configurations that make up the active LSCs using cells from #1

Material	**Quantity (S)**	**Quantity (M)**	**Quantity (L)**	**Source**
Polycarbonate	7680 g	9937.15 g	10603 g	*Desmet et al., 2012*
Lumogen F Red	3.3536 g	4.3392 g	4.6299 g	
Perylene Perinone	3.0208 g	3.9086 g	4.1705 g	
Stacked LSC sheets	256	16	4	
Nitrogen	-	-	-	*Han et al., 2013*
PET	883.2 g	1142.7 g	1219.3 g	
MCPET back reflector	256 x 2.5 cm^2	16 x 43 cm^2	4 x 220 cm^2	
LSC sheet	256	16	4	
PMMA	307.2 g	79.68 g	45.12 g	
PV cells (c-Si, 0.1 mm thick)	2560 cm^2	664 cm^2	376 cm^2	
Bison glue (acrylate ester)	512 ml	132.8 ml	75.2 ml	
LSC cells	256	16	4	

Table 4.4: Reactants and production steps to produce the sheets for LSC #2

Material	**Quantity**	**Source**
Reactants	Unknown	*None found*
Process energy	Unknown	
Product	CRS040	
	115.2 mg	
Material	**Quantity**	
Reactants	Unknown	*None found*
Process energy	Unknown	
Product	Lumogen F Red	
	384 mg	
Material	**Quantity**	
PMMA monomer	3465 g	*Wilson, 2010*
PMMA polymer	384 g	
Azubisisobutyronitrile	3.072 g	
Lumogen F Red	384 mg	
CRS040	115.2 mg	
Product	LSC Sheets (256)	
	5 x 5 x 0.5 cm $\rightarrow$ 6400 cm^2	

Table 4.5: Configurations that make up the active LSCs using cells from #2

Material	**Quantity (S)**	**Quantity (M)**	**Quantity (L)**	**Source**
PMMA monomer	3465 g	4483.4 g	4783.8 g	*Slooff et al., 2008*
PMMA polymer	384 g	496.9 g	530.2 g	
Azubisisobutyronitrile	3.072 g	3.975 g	4.241 g	
Lumogen F Red 305	384 mg	496.9 mg	530.2 mg	
CRS040	115.2 mg	149.1 mg	159.0 mg	
LSC sheets	256	16	4	
LSC sheet	256	16	4	
GaAs cell	640 cm^2	166 ^{2}	94 ^{2}	
Bison glue (acrylate ester)	256 ml	66.4 ml	37.6 ml	
Aluminium mirror (3 strips)	1920 ^{2}	498 ^{2}	282.0 ^{2}	
MCPET reflector	640 ^{2}	688 ^{2}	880 ^{2}	
LSC cells	256	16	4	

The different input materials to produce the waveguides and the luminophores for LSC #3 are similar to the input materials for LSC #2, the only difference being the amount of GaAs cells used on the edges, as this LSC cell has 4 GaAs cells on the sides instead of just one. Therefor the input materials for the waveguide and luminophores are not repeated and the following table shows the material inputs to produce the LSC cells.

Table 4.6: Configurations that make up the active LSCs using cells from #3

Material	**Quantity (S)**	**Quantity (M)**	**Quantity (L)**	**Source**
PMMA monomer	3465 g	4483.4 g	478308 g	*Slooff et al., 2008*
PMMA polymer	384 g	496.9 g	530.2 g	
Azubisisobutyronitrile	3.072 g	3.975 g	4.241 g	
Lumogen F Red 305	384 mg	496.9 mg	530.2 mg	
CRS040	115.2 mg	149.1 mg	159.0 mg	
LSC sheets	256	16	4	
LSC sheet	256	16	4	
GaAs cell	2560 cm^2	664 ^{2}	376 ^{2}	
Bison glue (acrylate ester)	1024 ml	664 ml	376 ml	
MCPET reflector	640 cm^2	688 cm^2	880 cm^2	
LSC cells	256	16	4	

Table 4.7: Reactants and production steps to produce the sheets for LSC #4

Material	**Quantity**	**Source**
CdO powder	0.365 g	*Xie et al., 2004*
Tetradecylphosphonic acid (TDAP)	1.5909 g	
Tributylphosphine oxide (TOPO)	28.41 g	
Argon flow	Unknown	
Se	0.0449 g	
Tributylphosphine (TBP)	14.2 g	
Methanol	106.53 g	
Toluene	Unknown (max 355.1 ml)	
Process energy	Unknown	
Product	CdSe core QDs	
	About 427.35 mg	
Material	**Quantity**	
ZnO	4.005 g	
Oleic acid	121.68 g	
1-octadecene (ODE)	354.42 ml	
Process energy	Unknown	
Product	0.1M Zn solution	
	492.25 ml	
Material	**Quantity**	
CdO	6.3185 g	
Oleic acid	121.68 g	
ODE	354.42 ml	
Process energy	Unknown	
Product	0.1M Cd solution	
	492.25 ml	
Material	**Quantity**	
Zn/Cd	3.8396 g	
Oleic acid	121.68 g	
ODE	354.42 g	
Process energy	Unknown	
Product	0.1M Zn/Cd solution	
	492.25 ml	

Table 4.8: Reactants and production steps to produce the sheets for LSC #4
Continued:

Material	**Quantity**	
ODE	59.07 ml	
Octadecylamine (ODA)	16.69 g	
CdSe QDs	427.35 mg	
0.1M Zn solution	Calculated amount	
0.1M Cd solution	Calculated amount	
0.1M Zn/Cd solution	Calculated amount	
Argon flow	Unknown	
Hexane	10 ml	
Methanol	Max 100 ml	
Process energy	Unknown	
Product	Completed QDs	
	3.328 μg	
Material	**Quantity**	
QDs	3.328 μg	*Bomm et al., 2011*
Monomer mixture of lauryl methacrylate (LMA)	4454.4 g	
Ethylene glycol dimethacrylate (EGDM)	1126.4 g	
Darocure © (UV-initiator)	5.632 g	
Process energy	Unknown	
Product	LSC sheets (256)	
	5 x 5 x 1 cm $\rightarrow$ 6400 cm^2	

Table 4.9: Configurations that make up the active LSCs using cells from #4

Material	**Quantity (S)**	**Quantity (M)**	**Quantity (L)**	**Source**
LSC sheets	256	16	4	*Bomm et al., 2011*
Multi-silicon solar cell	1280 cm^2	332 cm^2	188 cm^2	
Bison glue (acrylate ester)	256 ml	66.4 ml	37.6 ml	
LSC cell	256	16	4	

4.2.8 LSC module production

The previous section described the materials that are required to produce the different LSC cells as they have been found in literature. The next step is to incorporate multiple of these cells into a LSC module that can be used for BIPV. For this it is assumed that each of the modules will have a resemblance with the one illustrated earlier which was manufactured by Aste et al. and has been placed on a roof. With minor adjustments one could imagine such a module replacing a glass window or being applied in roofs to have natural lighting in a building. For this LCA study, BIPV modules of 1 m^2 are assumed. This means that some assumptions have to be made. It is assumed that the area not covered by LSC cells will consist of the aluminium frame. It also assumed that this frame will be 5 cm thick so that it can both incorporate the three layers (LSC, low-iron and regular soda-lime glass). The amount of aluminium required is assumed to be the average of the masses described for mounting structures of PV modules (Fthenakis et al., 2011). This is 1.4 kg/m^2 of module. This is then assumed to be 0.35 kg / side of the module. Thus, in order to produce 1m of framing of the required thickness, 0.35 kg of aluminium is required. It is assumed that the thickness is constant for the whole module and that the module can be described as a raster, and each line therefor requires 0.35 kg of aluminium. Thus the small cell module requires 34m of aluminium, the medium cell module requires 10m of aluminium and the large cell module requires 6m of aluminium.

In order to calculate the power output per module the electrical efficiency has to be calculated. This can be done based on the reported electrical efficiency in literature. The calculations for each of the 4 different BIPV modules are shown in Table 4.10 As a reference module the module constructed by Aste et al. is assumed. The efficiencies used in the table are efficiencies that are found in literature for small sized cells, therefor the efficiency is expected to be lower when considering larger cells. From these maximum power values it is chosen to have 8 x 1 m^2 of module per inverter.

Table 4.10: Showing the reported efficiencies and the associated maximum power for each LSC configuration under study.

	Comparison module	**#1**	**#2**	**#3**	**#4**
Reported efficiency (%)	1.26	4.2	4.6	7.1	2.8
Active area (m^2)	1.75	0.64	0.64	0.64	0.64
Maximum voltage (V)	24.29	-	-	-	-
Maximum current (A)	0.58	-	-	-	-
Maximum power (W)	14.08	26.88	29.44	45.44	17.92
Modules per inverter	-	9	8	6	13

Then, based on the expected power output of each module it is calculated how many modules have to be connected to a single 230W inverter to create an ideal set-up. This allows us to both divide the impact of the inverter and AC

cabling over the number of modules installed. Table 4.11 shows the calculations for the material requirements for each BIPV module consisting of small cells. Table 4.12 to 4.15 show the different configurations of the final modules.

Table 4.11: Calculations for the material requirements for each BIPV module consisting of small cells.

Material	**Quantity**
LSC cell (S)	256
Aluminium	11.9 kg
Low-iron soda-lime glass	6400 cm^2 x 6 mm
Regular soda-lime glass	6400 cm^2 x 4 mm
Tabbing	Cell dependent(4 per 5 cm PV side, 0.25 cm^2 each)
DC wiring (4 mm^2)	75 m
230 W Inverter	0.125
AC wiring (6 mm^2)	10 m

Table 4.12: Final configuration of a 1 m^2 of type #1.

Material	**Quantity (S)**	**Quantity (M)**	**Quantity (L)**	**Source**
LSC cell	256	16	4	Based on
Aluminium	11.9 kg	3.5 kg	2.1 kg	*Wilson, 2010*
Low-iron soda-lime glass (6 mm)	6400 cm^2	8281 cm^2	8836 cm^2	
Regular soda-lime glass (4 mm)	6400 cm^2	8281 cm^2	8836 cm^2	
Tabbing (4 per cell, 1 x 0.25 cm)	256 cm^2	64 cm^2	32 cm^2	
DC wiring (4 mm^2)	75 m	30 m	10 m	
AC wiring (6 mm^2)	Variable	Variable	Variable	
Inverter 230W	0.125	0.125	0.125	

Table 4.13: Final configuration of a 1 m^2 of type #2.

Material	**Quantity (S)**	**Quantity (M)**	**Quantity (L)**	**Source**
LSC cell	256	16	4	Based on
Aluminium	11.9 kg	3.5 kg	2.1 kg	*Wilson, 2010*
Low-iron soda-lime glass (6 mm)	6400 cm^2	8281 cm^2	8836 cm^2	
Regular soda-lime glass (4 mm)	6400 cm^2	8281 cm^2	8836 cm^2	
Tabbing (4 per cell, 1 x 0.25 cm)	256 cm^2	64 cm^2	32 cm^2	
DC wiring (4 mm^2)	75 m	30 m	10 m	
AC wiring (6 mm^2)	Variable	Variable	Variable	
Inverter 230W	0.125	0.125	0.125	

Table 4.14: Final configuration of a 1 m^2 of type #3.

Material	**Quantity (S)**	**Quantity (M)**	**Quantity (L)**	**Source**
LSC cell	256	16	4	Based on
Aluminium	11.9 kg	3.5 kg	2.1 kg	*Wilson, 2010*
Low-iron soda-lime glass (6 mm)	6400 cm^2	8281 cm^2	8836 cm^2	
Regular soda-lime glass (4 mm)	6400 cm^2	8281 cm^2	8836 cm^2	
Tabbing (4 per cell, 1 x 0.25 cm)	256 cm^2	64 cm^2	32 cm^2	
DC wiring (4 mm^2)	75 m	30 m	10 m	
AC wiring (6 mm^2)	Variable	Variable	Variable	
Inverter 230W	0.125	0.125	0.125	

Table 4.15: Final configuration of a 1 m^2 of type #4.

Material	**Quantity (S)**	**Quantity (M)**	**Quantity (L)**	**Source**
LSC cell	256	16	4	Based on
Aluminium	11.9 kg	3.5 kg	2.1 kg	*Wilson, 2010*
Low-iron soda-lime glass (6 mm)	6400 cm^2	8281 cm^2	8836 cm^2	
Regular soda-lime glass (4 mm)	6400 cm^2	8281 cm^2	8836 cm^2	
Tabbing (4 per cell, 1 x 0.25 cm)	256 cm^2	64 cm^2	32 cm^2	
DC wiring (4 mm^2)	75 m	30 m	10 m	
AC wiring (6 mm^2)	Variable	Variable	Variable	
Inverter 230W	0.125	0.125	0.125	

4.2.9 Conclusion

In this section an overview of the materials required to produce a BIPV LSC module has been given. Then the different amounts of input materials to produce 4 different modules based on 3 different sizes of cells are provided. These materials provide the input for the next subsection of chapter 4 which is the LCIA.

4.3 Life Cycle Impact Assessment (LCIA)

4.3.1 Impact of LSC modules

The estimated material quantities that were derived in section 4.2 have been used as input for the SimaPro software using the Ecoinvent database (Ecoinvent, 2007). By applying the IPCC 2007 GWP 100a emission set an environmental impact for the different configurations of LSC modules has been calculated. Table 4.16 gives an overview of the total impacts (inverter and wiring is already included).

Table 4.16: Environmental impacts of different module configurations and sizes.

Environmental impact (kg CO_2-eq)	**Module (S)**	**Module (M)**	**Module (L)**
Configuration #1	289.67	184.67	166.67
Configuration #2	229.67	135.67	116.67
Configuration #3	285.67	150.67	140.67
Configuration #4	234.67	140.67	121.67

Next to the impacts of the different modules, the impact for a 500W inverter (De Wild Scholten et al., 2006) and for 1 m of copper wiring has been derived from the Ecoinvent database (Table 4.17).

Table 4.17: Environmental impacts of copper wiring and a 500W inverter

Product	**Environmental impact (kg CO_2-eq)**
Copper wiring (1 m)	0.43
Inverter (500W)	36.1

For the modules that are installed as a BIPV solution it is assumed that 10m of wiring and 0.125 inverter is required to transport the produced electricity to the grid and no other combinations are assessed.

4.3.2 Cumulative energy demand and Wp of modules

Similar to how the environmental impact has been derived, the material inputs can also have their energy demand analysed by the SimaPro software. For this, the Cumulative Energy Demand method was chosen. Table 4.18 gives an overview of the total CED for the different modules (wiring and inverter included) and Table 4.19 for the wiring and inverter separately.

Table 4.18: Overview of the different CED values for the different LSC modules under study.

CED (GJ)	**Module (S)**	**Module (M)**	**Module (L)**
Configuration #1	4.87	2.94	2.61
Configuration #2	3.86	2.32	2.02
Configuration #3	4.88	2.59	2.16
Configuration #4	4.11	2.57	2.26

Table 4.19: CED of copper wiring and a 500W inverter

Product	**CED (MJ)**
Copper wiring (1 m)	7.88
Inverter (500W)	674

For the comparison of the various modules, the CED will be divided by the watt-peak (Wp). This is the maximum power under Standard Test Conditions (STC). To calculate the Wp for the LSCs under study the efficiency is multiplied with the cell area assuming an irradiation of 1000 W/m^2. An overview of the different Wp values is provided in Table 4.20. Due to the uncertainties associated with the efficiency of larger sized modules **(4.3.3)**, these are excluded when determining the CED/Wp ratio and only the small cell efficiencies are used.

Table 4.20: Wp for small modules for each configuration under study

Wp per module	**Module (S)**
Configuration #1	26.88
Configuration #2	29.44
Configuration #3	45.44
Configuration #4	17.92

4.3.3 Electrical output variations of the LSC modules

Before the expected electrical output can be compared to the environmental impact of the modules two aspects have to be taken into consideration. First, it is expected that the cell efficiency will decrease as the cell size increases, since due to the increased travel distance through the waveguide the photons have e.g. an increased chance of collision with a luminophore (self-absorption), are more absorbed by the waveguide material, and have an increased chance of escaping the waveguide before encountering the photovoltaic cells that are attached to the sides. Second, when considering conventional photovoltaics it is possible to place them in an ideal angle matching the incoming solar radiation to optimise the electrical properties. As it is assumed that the LSC modules are placed in buildings as a BIPV solution, this angle is unlikely to be achieved. Therefor

one has to consider the reduced electrical potential as a consequence of this installation limitations. This section aims to address both issues and provide realistic parameters that can be used to determine the environmental impact per amount of electricity that is produced under these assumptions.

Efficiency variations due to cell size variations

Not much studies have analysed how the electrical efficiency correlates with the size of the LSC cell. Two different types of studies have been found that give an indication of this correlation.

Sahin (2014) explains how Monte Carlo simulations for photon transport can provide insights in this matter. In this research it is first assumed that the PV cell covers a single edge and that only the length is varied. If this would be the case, the optimum performance (where the increase in light harvesting makes up for the decrease in efficiency) is found for a geometric factor (G) of 26, where G is the area of the surface facing the incoming radiation divided by the area of the side(s) with the photovoltaics attached. Thus the ratio between the surface area and the edge area provides a measure of estimating the gain of the LSC cell. However the cells that are the subject of this LCA study are squared instead of rectangular, and vary in the number of edges that are covered by a photovoltaic cell. Therefor it would prove difficult to provide realistic estimations on the expected change in efficiency solely based on this geometric factor. Based on the paper however one could assume that the medium cell could potentially have a slightly higher efficiency and the large cell would have a much lower efficiency compared to the small cells, thus indicating that the medium sized cells may have an higher electrical output.

Two other studies focus on the distance that the light has to travel through the waveguide before it reaches a photovoltaic cell and how this distance affects the edge output (Debije et al., 2009; Roncali et al., 1984). Results of their measurements are quite similar, as can be seen below (Figure 4.16). Here a large decrease in edge output is observed when shifting from small to medium squared cells and a smaller decrease is observed when shifting from a medium to large squared cell. However, one should also keep in mind that fluctuations could occur due to the difference in composition of each module, although it is realistic to assume that it would indeed resemble a decrease as is observed in these experiments as the travel distance through the waveguide is increased which results in an higher chance of losses associated with the waveguide and luminophores.

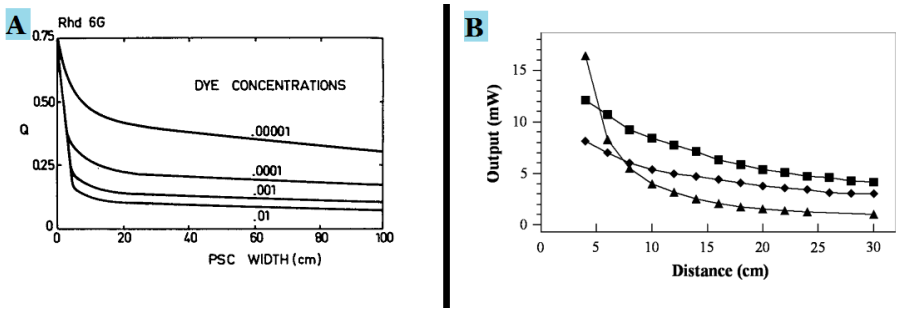

Figure 4.16: Graphs giving an indication of how the cell output could correlate with the cell dimensions. Study A compares different dye concentrations (Roncali et al., 1984); study B compares different cell shapes (Debije et al., 2009).

Due to the conflicting information and the unpredictability of the efficiency decrease, it is chosen in this research to work with various efficiencies based on the efficiencies found in the literature for each of the 4 modules that have had their LCI assessed. Three scenarios will be assessed. First it is assumed that the efficiency will stay the same for all of the three sizes. This could e.g. resemble an improved technology scenario. Second it is assumed that the decrease does indeed resemble a decrease as illustrated in Figure 4.16. Thus it is assumed that the efficiency is halved with each doubling in length. In the last scenario only the PBT of the smallest cell containing module is calculated and for the increasing areas there is no assumption made for the efficiencies, but calculations are made what efficiencies the modules should have in order to have the same PBT of the smallest cell module. For example, if a module with 4% efficiency would have an EPBT of 8 years, what is the minimum efficiency required for larger modules to have the same EPBT, and also being able to determine the likeliness of larger cell sizes having a shorter EPBT thus increasing their competitive position compared to the other modules. In all cases, the results should be interpreted carefully.

Efficiency variations due to orientation towards the sun

In the case of conventional PV the angle of the modules can be varied to ensure maximum exposure to the incoming solar radiation. When considering BIPV applications of LSC modules it is not possible to optimize this incoming radiation as the modules are fixed. In this study it is assumed that the modules are either installed on (or in) the building faade or in the roof. This placement affects the power output of the modules as the irradiation falling on the module becomes lower. It is suggested in literature (Batchelder et al., 1979) that in the case of LSC modules this can be explained by envisioning the loss in electrical output as a consequence of the decrease in area of the LSC which is proportional to the cosine function of the angle of incidence of the sunlight. Thus, since laboratory tests are often performed with an incoming solar radiation perpendicular

to the LSC module, in the case of BIPV it can be assumed that the efficiency of the cells is unchanged, but the total power output for the module decreases as the area receiving optimal irradiation decreases. For the Netherlands, the optimal tilt angle is 36°, for a south oriented panel (Figure 4.17).

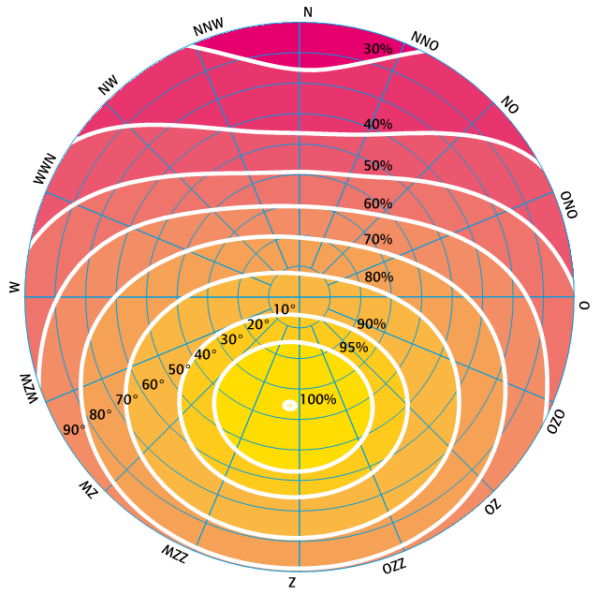

Figure 4.17: Angle and orientation dependency of maximum solar radiation in the Netherlands (Agentschap NL, 2010).

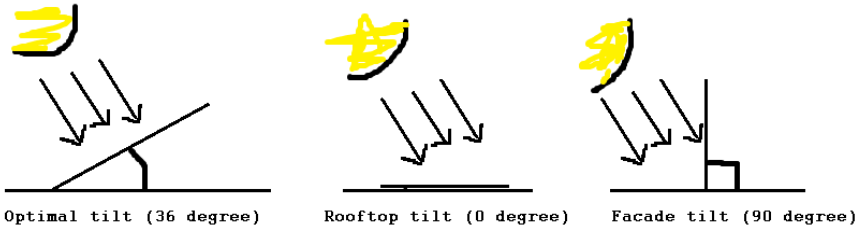

Figure 4.18: Illustration of the three different tilt angles considered.

The BIPV tilt angle is either 0° (roof integrated) or 90° (faade integrated) (Figure 4.18). This means an area decrease of 41.2% for faade BIPV and 19.1% for rooftop BIPV after correction (Figure 4.19). The optimal tilt angle, thus instalment under 36°, will also be considered for the environmental assessment, for the sake of convenience. In case of 0° the solar intensity on the panel is 90%, for 36° this is 100%, and for 90° this is 70%. The combination of both the

decrease of the LSC module area facing the sun perpendicular (Figure 4.19) and the decrease in solar radiation intensity will determine the amount of radiation that falls on the attached photovoltaic cells and can be converted to electricity.

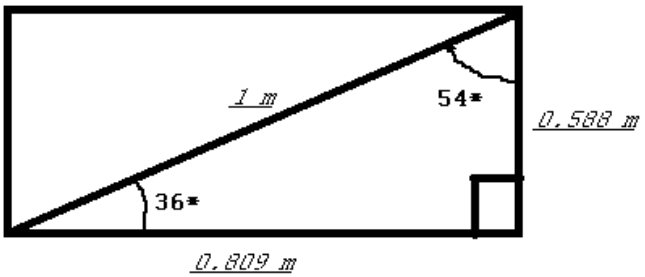

Figure 4.19: Illustration visualizing the reductions in power output due to sub-optimal orientation.

Temperature dependency of LSC modules and performance ratio

In a research conducted for the US government (Friedman, 1987) it is found that the temperature has a low effect on the efficiency of a LSC module. In the temperature range of 30 °C to 80 °C a small efficiency decrease of 5% was observed. In this experiment the photovoltaic cells were kept at 20 °C and only the waveguide was heated, but since in the assumed configuration of the modules that are the focus of this LCA the photovoltaic cells containing sides are sunk into the aluminium frame, one could say that they are to a certain degree shaded from the sun and the expected temperature rise will be much lower compared to sun facing photovoltaic cells. However temperature is only one part of the total performance ratio.

The performance ratio of a module is the observed electrical output divided by the best possible achievable output. This then provides an indication of the losses that occur in the various steps. In a study conducted on a large LSC module to determine the performance ratio it was found that the performance ratio on sunny days was 95% and the performance ration on cloudy days was 90% (Atse et. al., 2015). The authors have applied several uncertainty analysis from which they found that a maximum uncertainty of 5% would be the case. Despite spatial differences (the study has been conducted in Milan, Italy) it is assumed that a performance ratio of 90% is a valid choice to consider for the LCA on LSCs. This performance ratio is higher than the performance ratio found for other types of PV, e.g. for multi-Si PV a performance ratio of 75% is often found and is assumed as standard in literature (Fthenakis, 2011).

4.3.4 Comparison of impacts of LSC modules

Now that the different considerations that affect the environmental impact assessment are explained it is possible to calculate the values for the CO_2-eq/kWh, the impacts of the different components, the EPBT, and the CED/ Wp and CO_2 / Wp ratio under the assumption of a yearly average solar radiation of 1700 kWh/m^2 and an average solar radiation of 1100 kWh/m^2 which is the case in the Netherlands (Agentschap NL, 2010). Also the different orientations and different efficiencies will be taken into account, as elaborated on earlier. The performance ratio is assumed to be 90% and the lifetime of the modules is assumed to be 15 years, the primary energy equivalent of the electricity produced in Western Europe can be calculated from the average conversion efficiency of 0.31 (Fthenakis, 2011) meaning that in order to produce 1 kWh of electricity through the regular electricity grid 11.61 MJ of primary energy is required.

The following two graphs show CO_2-eq intensity of the modules per kWh of electricity produced assuming a lifetime of 15 years, both for an irradiation of 1100 kWh/m^2 and 1700 kWh/m^2. It is assumed that the efficiency decreases while increasing the size of the cells (mentioned in each graph). The purple line included in both graphs shows the CO_2-eq intensity of the best fossil energy source, which is gas at an intensity of 490 g CO_2-eq/kWh. These graphs allow to compare the LSC modules with this fossil energy source. As mentioned earlier, the environmental impacts of conventional PV is 29, 28 and 18 g CO_2-eq for mono-Si, multi-Si and CdTe respectively (lifetime of 30 years).

From the graph (Figure 4.20) it can be concluded that two out of four module configurations have sizes with an environmental impact lower than gas, #2 and #3. The other combinations perform worse than fossil gas, though it can be seen that #1 is in the proximity of 0.49. However all these modules have way higher environmental impacts compared to conventional PV. Even when a lifetime of 15 years is assumed for the conventional PV instead of 30 years, the worst environmental impact remains as low as 58 g CO_2-eq /kWh. If an irradiation of 1100 kWh/m^2 is assumed (Figure 4.21), only #3S and #3M at 36° and 0° are lower than gas, due to the high efficiency reported in literature for these modules. #1 and #2 are far from this level, suggesting that these configurations can only function environmental friendly in situations with high annual irradiation.

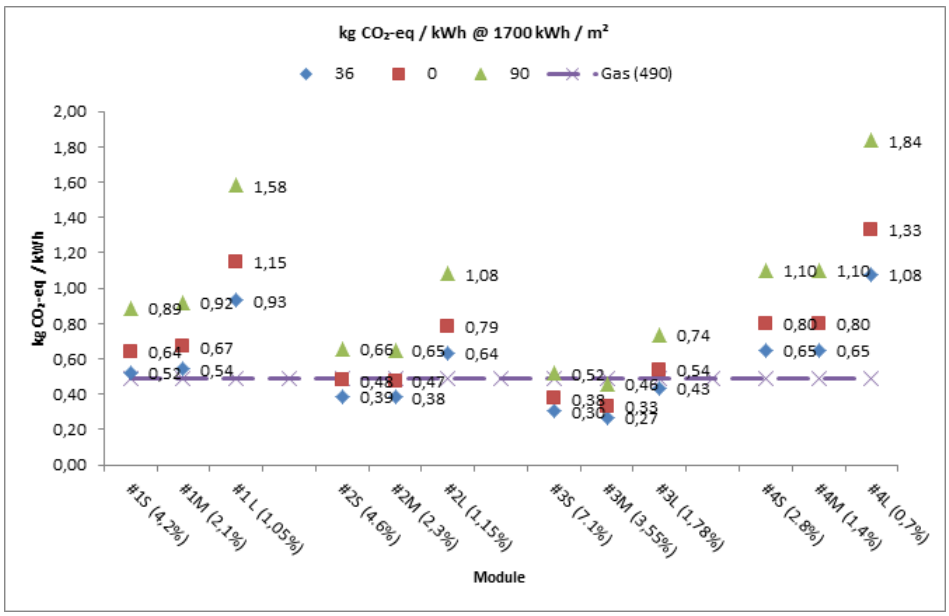

Figure 4.20: Graph showing the kg CO_2-eq / kWh for an irradiation of 1700 kWh / m^2 for the different modules and configurations.

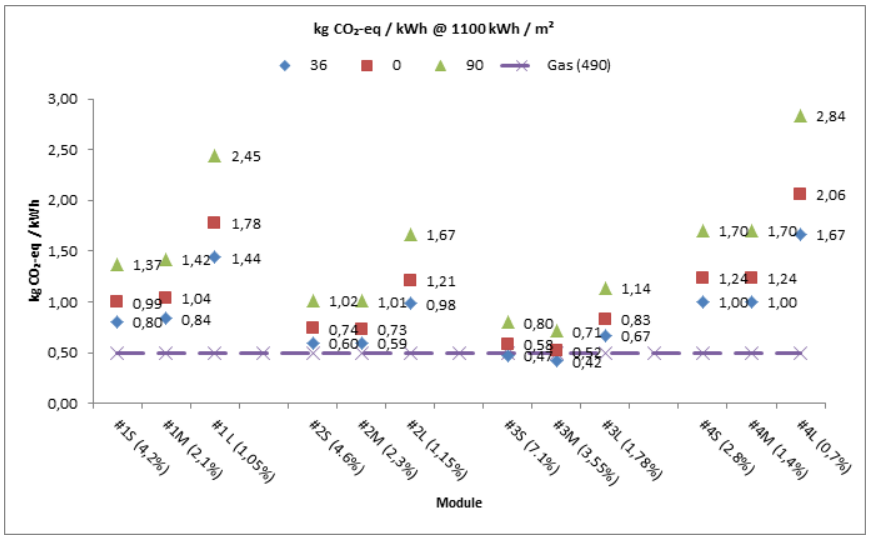

Figure 4.21: Graph showing the kg CO_2-eq / kWh for an irradiation of 1100 kWh / m^2 for the different modules and configurations.

The impacts can be divided over the different components that make up one module i.e. the waveguide and luminophores, the photovoltaic edge, the Al frame, and the BOS components (Figure 4.22). The CED ratios show that the CED of the Al frame is very significant when considering small cell modules. This becomes lower when shifting towards larger cell modules. The CED of the PV is only significant for the small cell modules, and becomes a very small fraction when moving to large cell modules, since the required PV is also dependent on the number of cells, more PV is required to cover edges of 256 small cells compared to only 16 medium cells or 4 large cells. The BOS CED starts to become more important when shifting to large cell modules, therefore a decrease in CED for these components can have larger impacts on these type of modules compared to small sized cells. In general, the CED graph indicates that by shifting to larger cells a decrease can be realized.

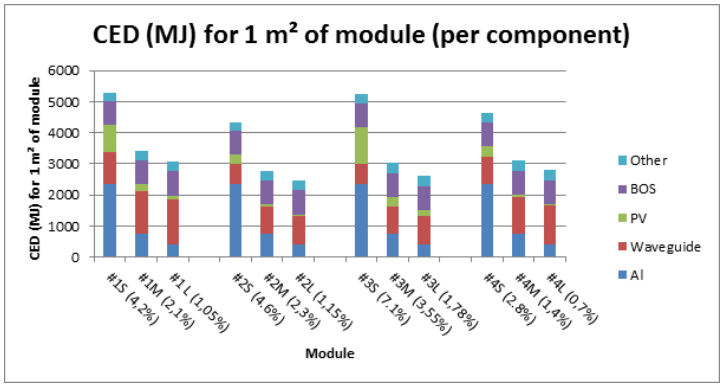

Figure 4.22: Graph illustrating the CED per component for the different modules and configurations.

Also, the total CO_2-eq impacts can be divided over the different components (Figure 4.23). Results are similar to the CED graph. What can be noticed when observing the CO_2-eq per m^2 of module is that for the small configurations the Al frame has by far the largest share in the total impact. When moving to larger cells sizes, thereby reducing the Al required, other components become more important, i.e. the waveguide. In general it is observed that the PV attached to the LSC cells always has a smaller impact, thus illustrating the benefit that LSC BIPV can have over conventional BIPV regarding the amount of photovoltaic cells required. The large cell modules have around 50% of the kg CO_2-eq/m^2 compared to their small cell counterparts.

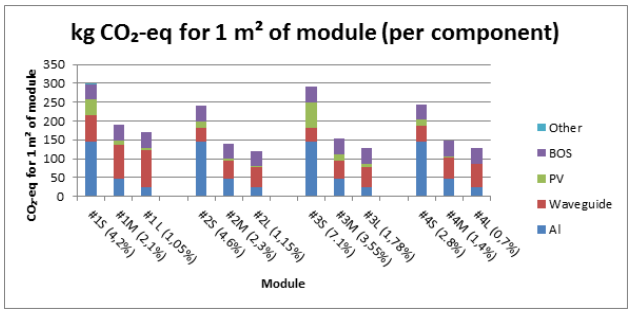

Figure 4.23: Graph illustrating the kg CO_2-eq / m^2 per component for the different module configurations.

From the previous results the EPBT can be calculated. First the comparison for the case of an annual irradiation of 1700 kWh /m^2 is looked into assuming a reduced efficiency as a consequence of the increase in size of the LSC cells (Figure 4.24). From this graph it is observed that the large cell modules have longer EPBTs compared to the small and medium sized modules. The best LSC configuration is again #3M (EPBT of 5 years). This graph also illustrates that the medium cells have a slightly lower EPBT compared to the small cells. When considering the lifetime of 15 years that is assumed for the modules, module configuration #1, #2, and #3 all show EPBTS of 10 years and lower, suggesting that these are able to produce more energy than is consumed during the fabrication when installed under 36°. However for BIPV it is more likely that the LSCs are installed at a 0° or 90° orientation, this graph then argues that a 0° orientation should be preferred over a 90° orientation, as the EPBTs can be around 30% longer for a 90° orientation.

In the case of an irradiation of 1100 kWh/m^2, which is the average value for e.g. The Netherlands, the EPBT becomes lower, though for some configurations the EPBT is still lower than the assumed lifetime of 15 years (Figure 4.25). Here, the best module is still #3M with an EPBT of 7.1 years at a 36° orientation and an EPBT of 8.8 years at 0° orientation. Also, both configuration #2 and #3 show promising EPBTs at this irradiation level, especially when compared with #1 and #4, suggesting that these can find applications as BIPV in less sunny regions such as The Netherlands.

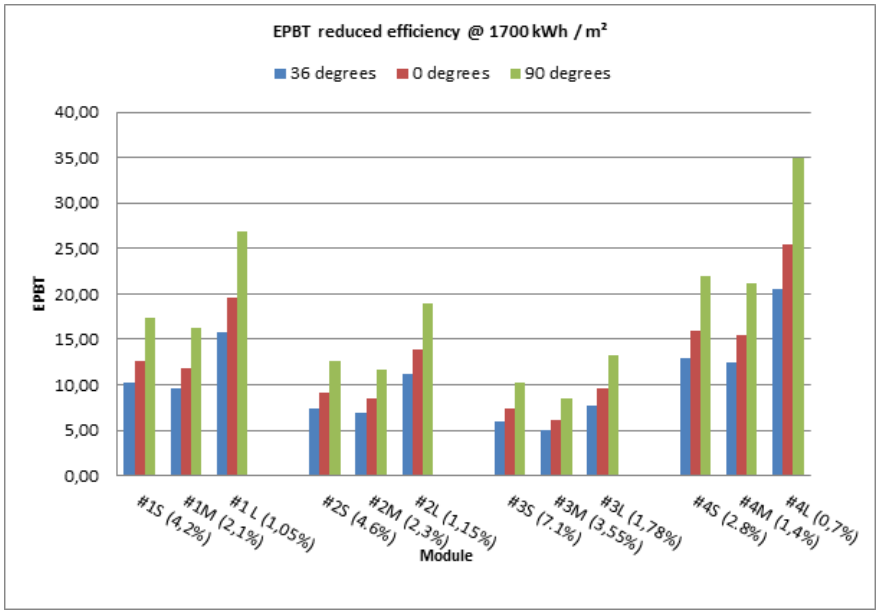

Figure 4.24: Graph showing the EPBTs for the different modules and configurations under an irradiation of 1700 kWh/m^2.

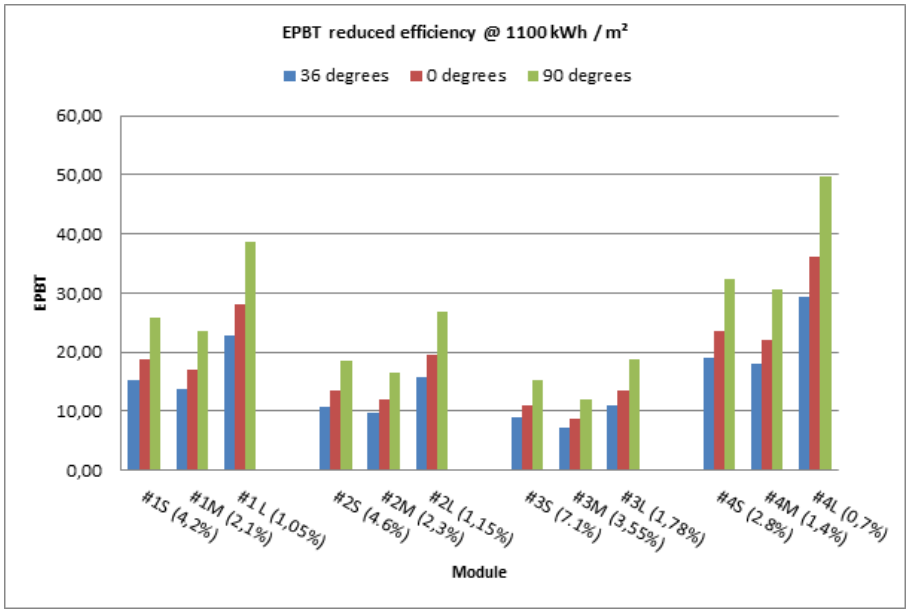

Figure 4.25: Graph showing the EPBTs for the different modules and configurations under an irradiation of 1100 kWh / m^2.

The CO_2-eq/Wp is another value that can be used to compare various electricity sources (Figure 4.26). In the graph these values are illustrated for the small cell modules, as these Wp values are the most reliable as no assumptions for the reduced efficiencies had to be made. From this graph it can be seen that, similar to the other comparisons, module #3M shows the best value with a kg CO_2-eq/Wp value of 6.29.

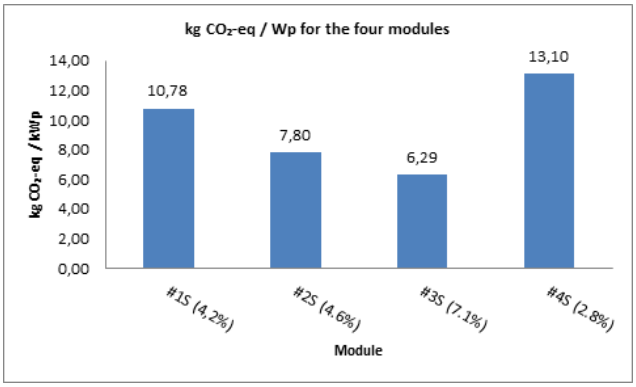

Figure 4.26: Graph showing the kg CO_2-eq/Wp for the four module configurations using small cells.

The other graph (Figure 4.27) shows the CED/Wp ratio. This is an advisable ratio from an energy efficiency perspective, as it incorporates the differences in conversion efficiency (Laleman et al., 2013). Compared to conventional PV, the CED/kWp ratios for LSCs are much higher. From literature it is found that mono c-Si has a CED/Wp ratio of 37 and multi c-si has a CED/Wp ratio of 31. Here the best CED/Wp value is again found for module #3M, 107.37.

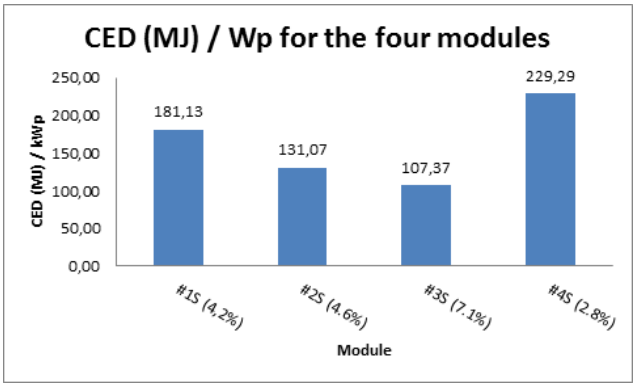

Figure 4.27: Graph showing the CED/Wp in MJ for the four module configurations using small cells.

Chapter 5

Sensitivity and uncertainty analysis

In order to interpret the results from the LCA study more careful it is possible to conduct both a sensitivity and uncertainty analysis to see how the results that were found earlier depend on the different inputs. This can be done by varying the parameters. In a sensitivity analysis the focus is on how sensitive the final result correlates with an assumed value for certain products and processes. If other materials or other frame dimensions are chosen, how would the outcome change. For the uncertainty analysis, one has to find the uncertainties in the research and see how the upper and lower boundaries of this uncertainty alter the final outcomes. All module configurations are assessed, but the focus is only on the 36° orientation with an annual irradiation of 1700 kWh/m^2 . This is done for three reasons. First, this orientation has the best electrical output, therefor it is thought that the correlation of the changing impacts and the electrical output has the highest sensitivity for this orientation. Second, the higher annual irradiation resulted in several module configurations and sizes having kg CO_2-eq/kWh values already close or below the value for fossil gas electricity generation, whereas an irradiation of 1100 kWh/m^2 would require more drastic changes in the impact to achieve similar values, thus the focus here is only on the 1700 kWh/m^2 value to see how the sensitivity links to this value of 0.49 kg CO_2-eq/kWh. Last, to be able to present the results clearly the aforementioned choices result in visually less complex graphs.

5.1 Sensitivity analysis

The sensitivity depends on the materials used and the assumed quantities of the materials required in order to produce the modules under study. In order to calculate the sensitivity the inputs have to be altered. The starting point is the value that is deemed to most plausible. Then, the value can be altered to include e.g. the minima and maxima or the parameter can be doubled or

halved. If during the sensitivity analysis results show only marginally variations, an approximate value can be found appropriate, but when the results show significant variations, the parameter should be accurate.

5.1.1 Aluminium frame

The component having the largest share in the environmental impact is the aluminium frame. This means that the results depend heavily on the assumptions made when determining the amount of aluminium required, especially in the case of small modules. In the LCI the amount of aluminium required has been determined from different types of conventional PV modules, and the average value for different mounting structures was used (e.g. rooftop, building integrated). For the sensitivity the amount required is altered, as it is possible that building integrated LSC modules require more or less aluminium compared to conventional PV due to various differences such as weight and vulnerability. In order to assess the sensitivity of the aluminium both a 25% reduction and increase in material and processing energy required is assumed and the dependency of the PBTs and the CO_2-eq/kWh on this value is assessed.

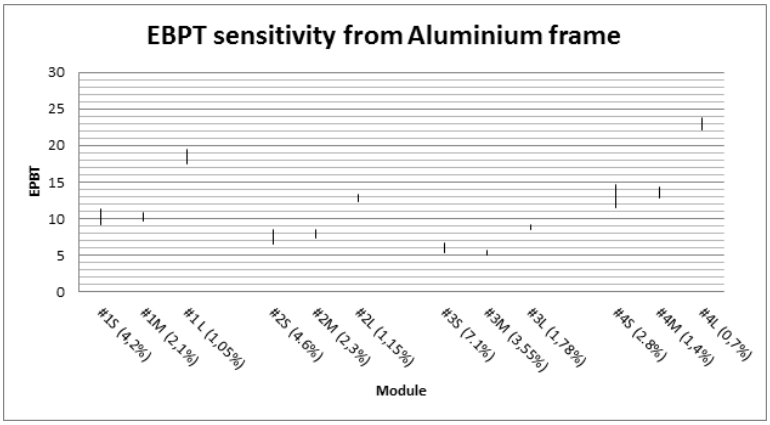

Figure 5.1: Graph illustrating the EPBT sensitivity from the variations in the aluminium frame.

What can be observed from the variety in EPBTs (Figure 5.1) is that the largest sensitivity of the modules on the amount of aluminium used is found in the small modules. This can be explained by the fact that the small modules have the largest amount of aluminium compared to the other modules. It is also found that module #4 is more sensitive to the change in aluminium compared to #1, #2, and #3. This is due to the lower efficiency of module #4. For module configuration #3 the sensitivity of the EPBT relative to the aluminium used is marginal due to the high efficiency of the cells. Regarding the CO_2-eq/kWh values (Figure 5.2) only marginal changes are observed, again showing that the change in aluminium only has larger effects in lower efficiency modules.

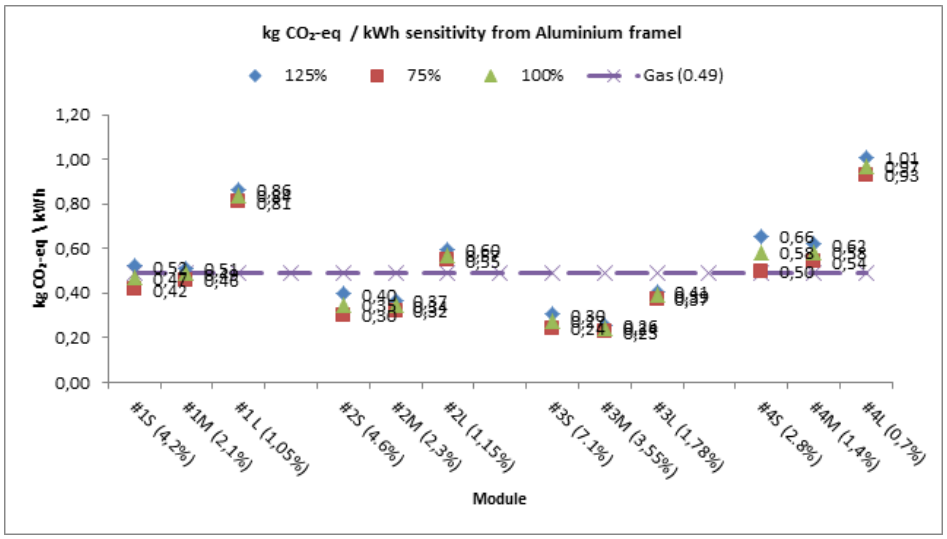

Figure 5.2: Graph illustrating the kg CO_2-eq/kWh sensitivity from the variations in the aluminium frame.

5.1.2 Chemicals

As some of the LSCs require rather specific chemicals, these were not available in the database. This was often the case for the luminophores, as the chemical processes or structures are patented, and certain reactants for the waveguide material were lacking. If this was the case chemicals which did show similar characteristics or had the same functional groups (when organic chemicals were used) have been used as a substitute. This different choice of chemicals also results in a different value for the environmental impacts. In order to assess the sensitivity of the PBTs on the chemicals used all modules will have their waveguide and luminophore impacts increased and decreased by 25%.

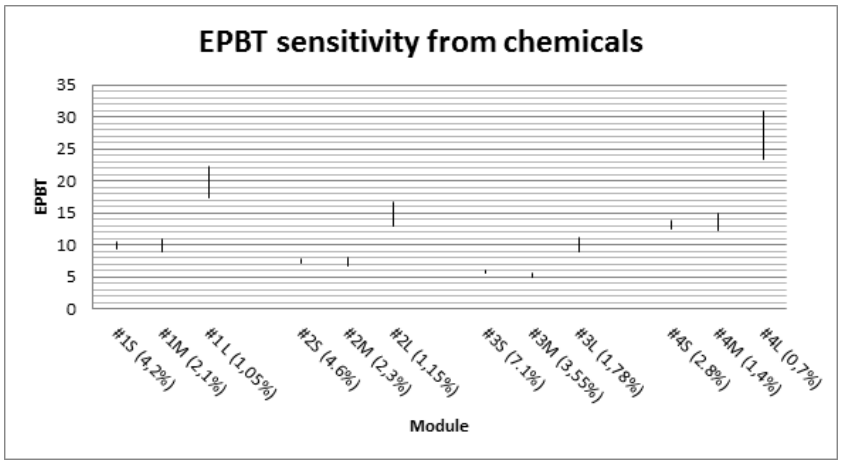

Figure 5.3: Graph illustrating the EPBT sensitivity from the variations in the chemicals.

It can be seen from the sensitivity analysis that the EPBT is the most sensitive to changes in the chemical requirements when large LSC modules are considered (Figure 5.3). This is due to the larger share of the chemicals compared to the other components, which can be as high as 50% in the case of configuration #1 and #4, since the increase in waveguide when moving to larger cells results in a decrease in aluminium required, which has a large environmental impact. Looking at the kg CO_2-eq/kWh graph (Figure 5.4) it can be seen that an increase of 25% of the chemicals does not result in the modules which already had an CO_2-eq/kWh requirement lower than gas to become suddenly higher than gas, but it is observed that a decrease of 25% of the chemicals causes the small and medium modules of configuration #1 to become favourable over gas.

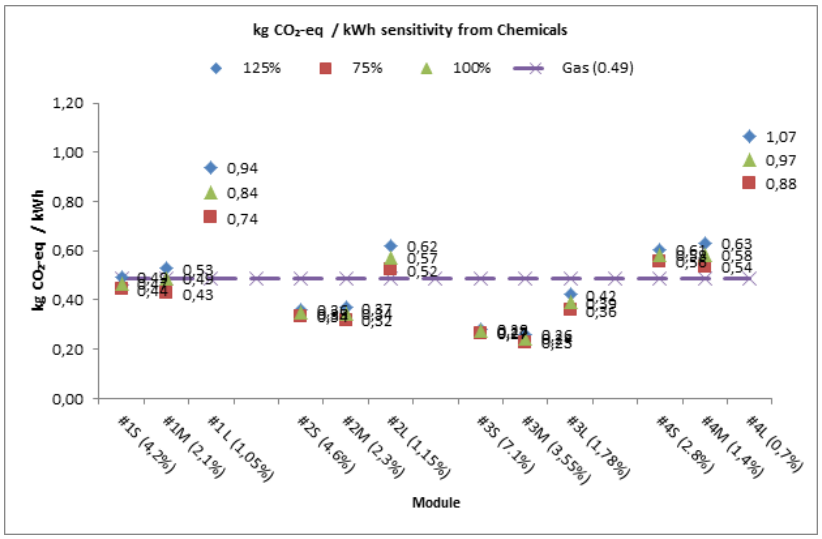

Figure 5.4: Graph illustrating the kg CO_2-eq/kWh sensitivity from the variations in the chemicals.

5.1.3 Energy

For the LCA study several energy factors are used as an input. These energy factors were general factors e.g. for the production of plastic and moulding of aluminium. As the sensitivity for aluminium is already covered earlier as included in the aluminium sensitivity, here the focus is on the energy required for the plastics. It is possible that a specific type of plastic requires more or less energy than the other. In order to quantify this, the energy required is also increased and decreased by 25% to see how this impacts the results.

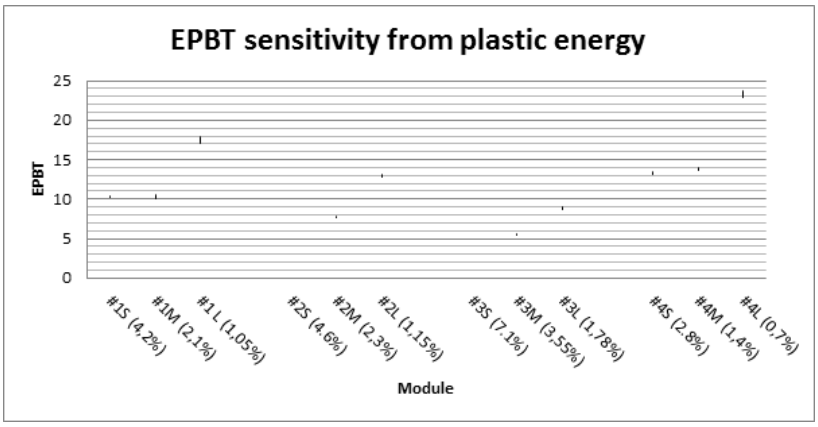

Figure 5.5: Graph illustrating the EPBT sensitivity from the variations in the plastic energy.

What can clearly be seen is that the impact of the plastic is a very small component of the total impact (figure 5.6) and that both an increase and decrease of this value hardly affect the EPBTs. As a similar result, the kg CO_2-eq/kWh also does not significantly change (figure 5.7). Although the plastics represent a large part of the materials used, especially in the larger modules, the energy is a smaller fraction of this total impact.

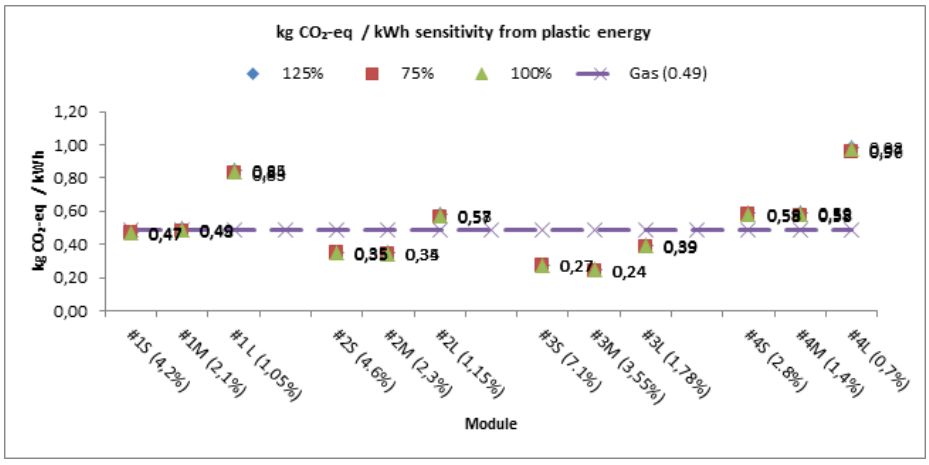

Figure 5.6: Graph illustrating the kg CO_2-eq/kWh sensitivity from the variations in the plastic energy.

5.1.4 Total Sensitivity

Finally, it is possible to sum up all the previous sensitivity analysis in one final analysis, that is increase and decrease all the factors described above by 25% to see how a module that requires 25% less on these factors performs and how a possible increase of 25% affects the outcome of the analysis. This could represent a certain upper and lower boundary to the PBTs.

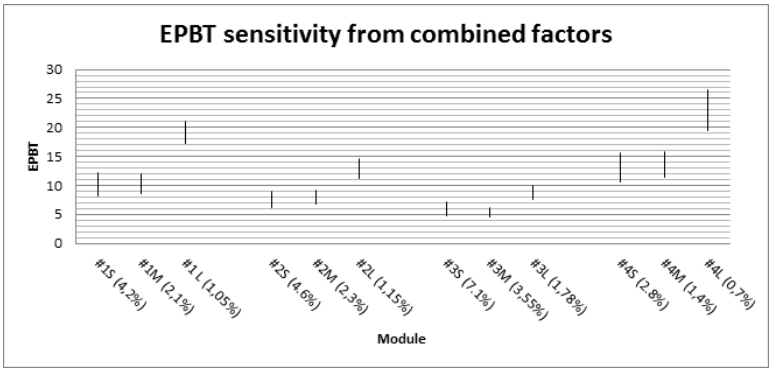

Figure 5.7: Graph illustrating the EPBT sensitivity from the variations in the combined factors.

From the sensitivity of the EPBTs (Figure 5.7) it can be observed that the large cell modules tend to show a stronger sensitivity to the total sum of parameters that are altered. The medium cell modules slow the smallest variations, suggesting that for these combination of components the sum of impacts has a certain balanced effect. Interesting to see is that in the case of the CO_2-eq/kWh (Figure 5.8) all modules, when assuming the situation with lower impacts than the standard scenario, show values below the fossil gas electricity line, with the exception of #1L and #4L. This shows that if energy efficiency and material intensity can decrease to around 75% of what is used now, all modules can end up in the greener regions of the electricity generating options available. One should however still consider that these are higher compared to conventional PV, thus good arguments should be used to choose one option over the other.

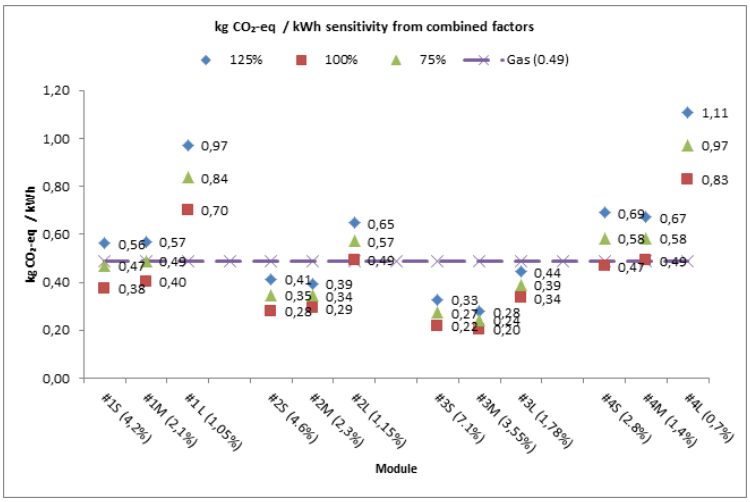

Figure 5.8: Graph illustrating the kg CO_2-eq/kWh sensitivity from the variations in the combined factors.

5.2 Uncertainty analysis

Several assumptions have been made that affect the overall performance of the modules, such as the lifetime and the performance ratio. These assumptions include a certain uncertainty as these values are often derived from second sources and thus cannot be directly linked to the individual modules. By acknowledging these uncertainties and specifying a range of uncertainty for these different factors it is again possible (similar to the sensitivity analysis) to see how the uncertainties affect the PBTs and the CO_2-eq/kWh. The various uncertainties are discussed below.

5.2.1 Performance ratio

The performance ratio has been set at 90%. However this is backed up by only one source. Conventional PV has a lower performance ratio. For rooftop mounted PV a performance ratio of 75% can be assumed (Fthenakis, 2011). Therefor it is useful to see how a lower performance ratio affects the PBTs.

What can be seen from the EPBTs graph (Figure 5.9) is that the performance ratio has larger impacts when shifting to larger modules. This can be explained by the fact that these modules have a larger area consisting of cells compared to the small and medium modules. In general it can be stated that the uncertainty associated with the performance ratio results in EPBTs that are 2 to 3 years longer in case of small and medium modules and as much as 5 years in large modules. Thus, if LSCs do indeed have a performance ratio of 75%, this would have a significant effect, thus suggesting that extra research into the performance ratio is validated.

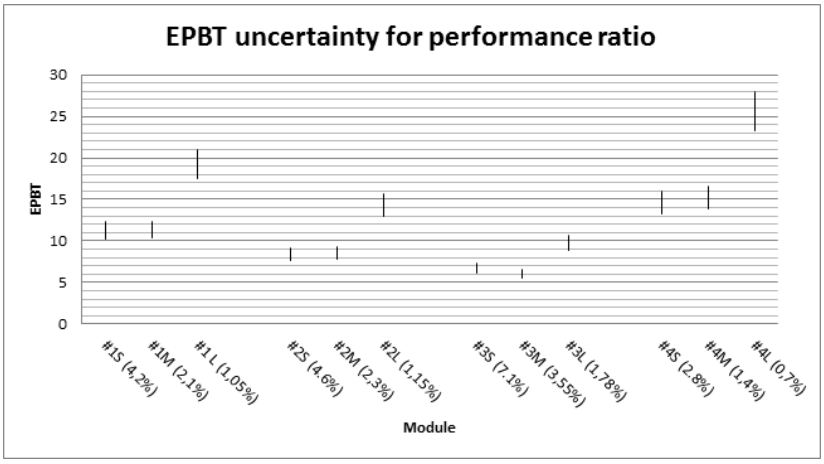

Figure 5.9: Graph illustrating the EPBT uncertainty caused by the performance ratio.

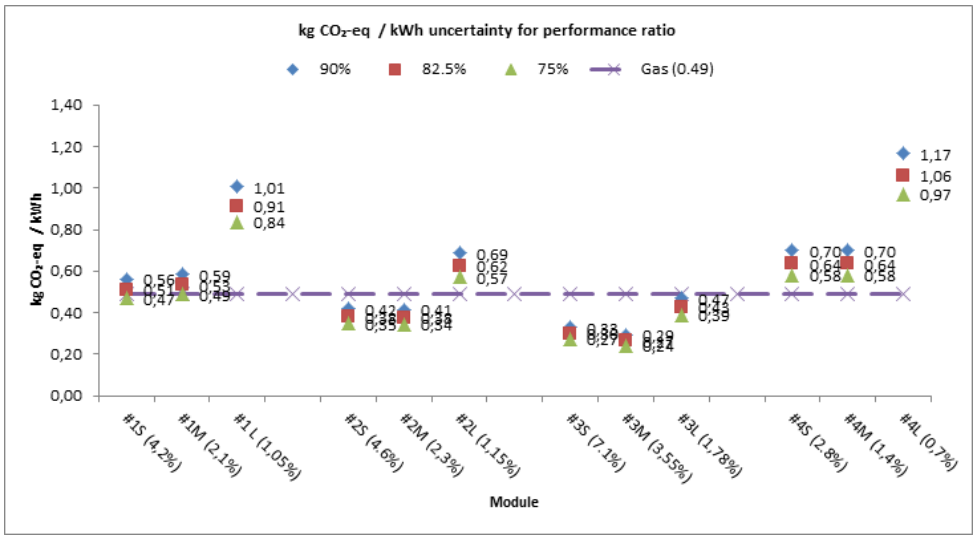

Figure 5.10: Graph illustrating the kg CO_2-eq/kWh uncertainty caused by the performance ratio.

The same can be said for the CO_2-eq/kWh impacts. Again there is a larger uncertainty observed in the large cell modules and a smaller uncertainty in the small and medium cell modules. Only in the case of #1S and #1M does this result in a shift from below 0.49 kg CO_2-eq/kWh to a larger value.

5.2.2 Lifetime

The assumed life for the building integrated LSC modules is 15 years. However conventional PV can have a lifetime of up to 30 years. If the LSC modules do have a longer lifetime, the amount of electricity generated over time would increase and the associated environmental impact per kWh will decrease. If this is the case, it would be more attractive to install these modules. Therefor the uncertainty of the lifetime has to be acknowledged. The EPBT does not depend on the lifetime, therefore only the CO_2-eq/kWh is assessed.

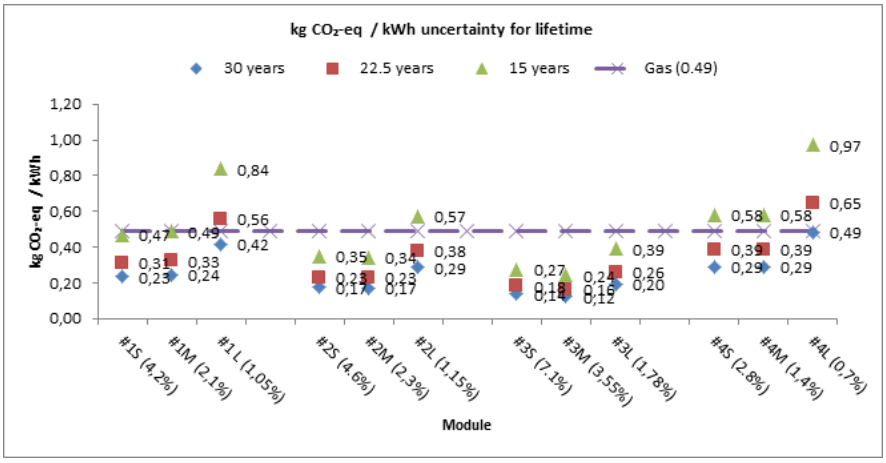

Figure 5.11: Graph illustrating the kg CO_2-eq/kWh uncertainty caused by the lifetime.

What can be observed when looking at the results of the variation in lifetime (Figure 5.11) is that when a lifetime of 30 years is assumed, all modules have impacts lower than fossil gas. Though still not comparable with conventional PV, the more efficient modules, see their impacts greatly reduced to an even more lower value. It is debatable how likely the lifetime of LSCs will increase in the future, however here it is illustrated that increasing the lifetime can have a large impact in the overall goal of achieving lower impacts, especially when combined with higher electrical conversion efficiencies.

5.2.3 Surface area covered by cells

The assumption has been made that in the case of small modules only 0.64 m^2 of the 1 m^2 module is covered by LSC cells. This is less compared to e.g. the large

cells, where a larger area is covered by LSC cells, albeit with a smaller efficiency. This assumption affects both the electricity output that can be realised and the aluminium that is required for the modules. This uncertainty is tested by increasing the cell area covered by 5% and 10% for all cell sizes, and decreasing the aluminium required by 5% and 10% simultaneously, to see how this affects the PBTs and the CO_2-eq/kWh.

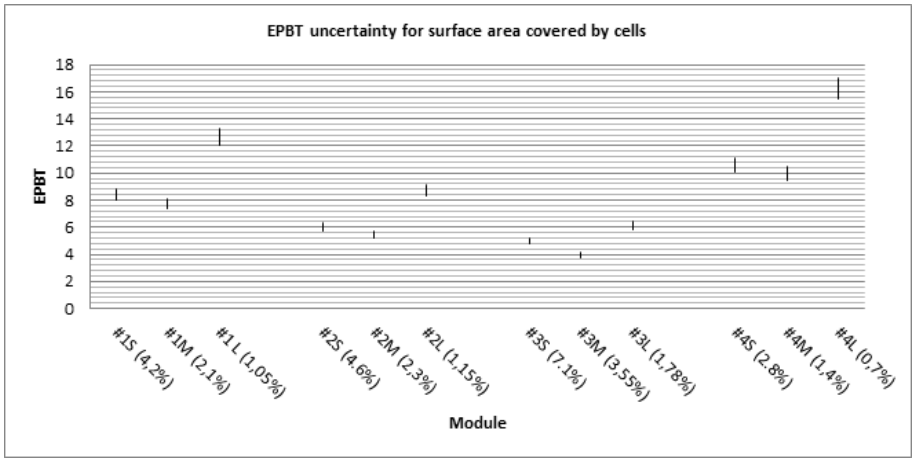

Figure 5.12: Graph illustrating the EPBT uncertainty caused by the surface area covered by cells.

From the EPBTs graph it can be seen that in the case of larger cells there is more dependency on the module area covered by cells when compared to small and medium sized cells, especially in the case of configurations #1 and #4 (Figure 5.13). This can be explained by two reasons. First, a 5% increase in the larger cells results in a larger difference of surface area compared to a 5% increase in the small cell module surface area. Though the aluminium is higher in the small cell modules, a 5% decrease is not that much to see the effects on the EPBT. The increase in surface area on large modules however, combined with the lower CED of these modules, results in more decrease in EPBTs as the higher electricity generated has a lower CED to compensate for. Second, and this applies to all sensitivities and uncertainties, is that configuration #1 and #4 have larger CEDs than configuration #2 and #3, thus any decrease in materials used has a larger effect on the EPBTs. It is easier to spot big changes in big numbers compared to small changes in small numbers. The CO_2-eq/kWh shows that an increase in surface area results in a slightly lower value (Figure 5.14). No significant changes occur here, as no module or configuration crosses the 0.49 kg CO_2-eq/kWh barrier.

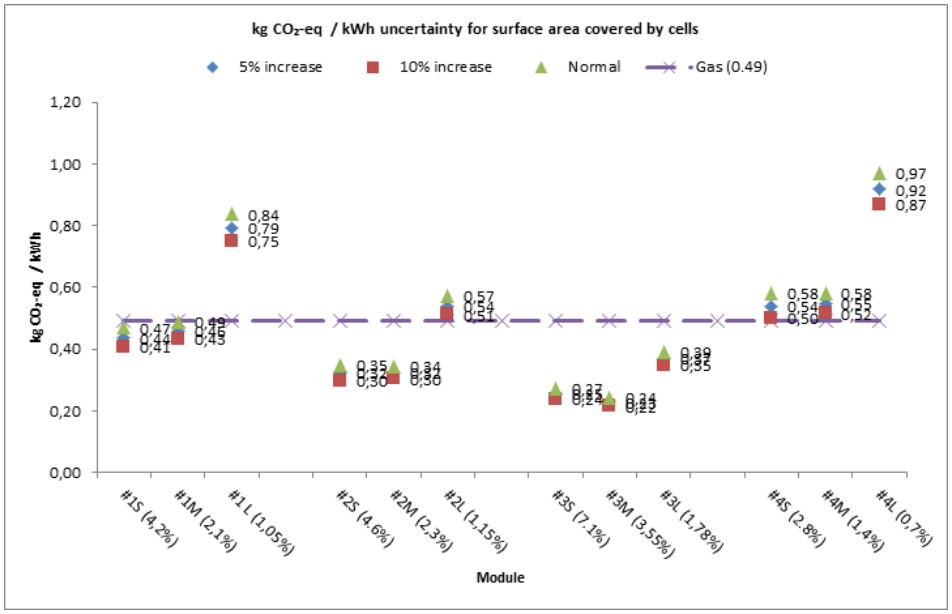

Figure 5.13: Graph illustrating the kg CO_2-eq/kWh uncertainty caused by the surface area covered by cells.

Chapter 6

Discussion and conclusion

6.1 Discussion

From the different LCA categories which assessed the various configurations and sizes of building integrated LSC modules it can be said that configuration #3 has the shortest EPBT and the lowest CO_2-eq/kWh. Large variations are observed when comparing the different angles at which the modules are installed. Slightly tilted shows the most promising PBTs, thus suggesting that sloped application may be favoured over vertical or horizontal application. If sloped application is not possible rooftop application is favoured over façade application, as this has a better PBT.

The EPBT graphs presented in the sensitivity analysis all assume a irradiation of 1700 kWh/m^2. In e.g. The Netherlands, annual irradiation is lower, thus causing a longer PBT for the modules presented. This suggests that application in regions with lower irradiation intensity is not feasible at this moment, as the reduction in irradiation causes the PBT of the modules to be at least 30% longer. An increase in efficiency is therefore required to allow for installation in more regions around the world.

Several other assumptions are made during this research that affect the observed PBTs. First, some materials used in literature could not be found in the Ecoinvent database, more specifically waveguide and luminophore materials. If this was the case comparable materials were chosen, but these have different intensities. However as is shown in the graphs the waveguide (which includes the luminophores) have a small share in the total energy and CO_2-eq intensity when compared to the total intensity of the small cell sized modules. Only when moving to larger cells this uncertainty starts to become more important. Second, as the efficiencies for larger cells had to be estimated these values become more uncertain. It is assumed that the reduction in efficiencies does follow a similar pattern, but the exact efficiencies remain uncertain. However as the overall energy and CO_2 intensity becomes smaller, the PBTs become less dependent on the efficiencies, thus one could argue that the observed PBTs are

more or less representative. Third and most important are the lifetimes of the modules. So far most papers indicate that their cells are stable for at least 5 years, however far longer lifetimes are required in order to complement the PBTs found in this LCA study. Especially when shifting to larger modules the relative importance of the cells starts to increase as they also become a large part of the overall intensities. Most of these variations have been assessed in the sensitivity and uncertainty analysis however it should be mentioned that these analysis have been more illustrative than quantitative as there are many more factors which could have been picked to end up with even more considerations and parameters that should be acknowledged. Nevertheless, the lifetime thus remains an important focus point for future research, as well as efficiency improvement and large module testing to get more ideas on the performance ratio, though an efficiency of 7.1% appears to be quite useful already for BIPV applications of LSCs. Combined with the decreased costs of these modules due to up-scaling of active area while downscaling the costs of the photovoltaic cells, one can envision applications in the near future.

Another focus point for future research could be on the possibilities of recycling of certain components of the LSCs. If certain parts could last for multiple module cycles the relative intensity of these components becomes smaller. This is especially the case for the aluminium frame. If it would be possible to keep the frame in place and only replace the LSC cells once their lifetime expires the PBT of the small cells containing module could decrease dramatically. It is also important to take into account the energy and CO_2 intensity of the building materials that are replaced by the modules, e.g. bricks, window panes and roof tiles. Several values for these materials can be found in literature. A window with a lifetime of 75 years and a size of 600 x 1200 mm (Salazar et al., 2008) is found to have an impact of 341 kg CO_2 for aluminium-clad windows, 456 kg CO_2 for PVC windows and 357 kg CO_2 for fiberglass windows. These values would indicate that a module could be favoured over a regular window, especially when considering the energy that can be produced simultaneously.

It could be useful to investigate the heat transfer through the modules to see if they are comparable to double glazing or triple glazing. If this is the case the installation of LSC modules could find another incentive in the fact that the overall heat demand of the building decreases, next to aesthetics this is an important factor architects and constructers take into consideration.

Finally, a topic that has not been touched upon in this research is what happens to the modules during the disposal phase. It could for example be attractive to try and re-use the aluminium frame and only replace the LSC cells. Also, as the waveguide often is a plastic like any other, it could be re-used to fabricate other products, such as benches. By maximizing the re-use potential during the material selection and manufacturing stages the total environmental impacts can be reduced even more.

6.2 Conclusion

The aim of this research was to answer the previously stated research question:

> What is the environmental impact of LSCs.

In order to answer this question first a literature study has been conducted to find out what materials make up a LSC module. Then, several configurations and sizes of BIPV LSC modules have seen their energy and CO_2-eq/kWh intensity determined using the SimaPro software and the Ecoinvent databse. From this analysis, it is found that the best EPBTs are resulting from module configuration #3M. The other sized cells of #3 perform better than the other module configurations and sizes. The second best is module configuration #2 followed by #1, and #4 has the longest EPBTs. This correlates with the different efficiencies reported in literature for the small sized cells. From the comparison between the different components that make up the module it can be concluded that the aluminium frame has a large share in the overall environmental footprint. For modules consisting of larger sized cells this shifts towards the waveguide and BOS components having equally large shares. Sloped orientation still proves to be the best orientation, however roof placed or façade placed BIPV LSC applications can be considered in a region with large solar irradiation and to a lesser extent in a region with smaller solar irradiation. For module configuration #3M this would result in a EPBT of 5 to 7.8 years and a kg CO_2-eq/kWh of 0.27 to 0.43.

Bibliography

[1] Agentschap NL (2010) Leidraad Zonnestroomprojecten. Retrieved from http://www.rvo.nl/sites/default/files/bijlagen/Leidraad%20Zonnestroomprojecten.pdf

[2] Aste N., Tagliabue L.C., Del Pero C., Testa D., Fusco R. (2015) Performance analysis of a large-area luminescent solar concentrator module. *Renewable Energy*, 76, 330-337. doi: 10.1016/j.renene.2014.11.026

[3] Batchelder J.S., Zewail A.H., Cole T. (1979) Luminescent solar concentrators. 1: Theory of operation and techniques for performance evaluation. *Applied Optics*, 18(18), 3090-3110

[4] Bomm J., Bchtemann A., Chatten A.J., Bose R., Farrell D.J., Chan N.L.A, Xiao Y., Slooff L.H., Meyer T., Meyer A., Van Sark W.G.J.H.M, Koole R.(2011) Fabrication and full characterization of state-of-the-art quantum dot lu-minescent solar concentrators. *Solar Energy Materials* & Solar Cells, 95, 2087-2094. doi:10.1016/j.solmat.2011.02.027

[5] Braun D., Cherdron H., Rehahn M., Ritter H., Voit B., (2012) Polymer Synthesis: Theory and Practice. New York, NY: Springer

[6] Bauhuis G.J., Mulder P., Haverkam E.J., Huijben J.C.C.M., Schermer J.J. (2009) 26.1% thin-film GaAs solar cell using epitaxial lift-ff. *Solar Energy Materials* & Solar cells, 93, 1488-1491. doi: 10.1016/j.solmat.2009.03.027

[7] Ceccaroli B., Lohne O. (2011). Solar Grade Silicon Feedstock. In A. Luque & S. Hegedus (Eds.), Handbook of Photovoltaic Science and Engineering (pp. 169-215). West Sussex, UK: John Wiley & Sons Ltd.

[8] Chapin D.M., Fuller C.S., Pearson G.L (1954) A New Silicon p-n Junction Photocell for Converting Solar Radiation into Electrical Power. *Journal of Applied Physics*, 25, 676-677. doi: 10.1063/1.1721711

[9] De Wild - Scholten M.J., Alsema E.A., Ter Horst E.W., Bchler M., Fthenakis V.M. (2006) A Cost and Environmental Impact Comparison of Grid-Connected Rooftop and Ground-Based PV Systems. European Photovoltaic Solar Energy Conference, September 4th - 8th, 2006, Dresden, Germany.

[10] Debije M.G., Teunissen J.P., Kastelijn M.J., Verbunt P.P.C., Bastiaansen C.W.M. (2009) The effect of a scattering layer on the edge output of a luminescent solar concentrator. *Solar Energy Materials* & Solar Cells, 93, 1345-1350. doi: 10.1016/j.solmat.2009.02.013

[11] Debije M.G., Verbunt P.P.C., Nadkarni P.J., Velate S., Bhaumik K., Nedumbamana S., Rowan B.C., Richards B.S., Hoeks T.L. (2011) Promising fluorescent dye for solar energy conversion based on a perylene perinone. *Applied Optics*, 50(2), 163-169

[12] Debije M. G., Verbunt P. P. C. (2012), Thirty Years of Luminescent Solar Concentrator Research: Solar Energy for the Built Environment, *Advanced Energy Materials* Vol. 2 p12 35

[13] Desmet L., Ras A.J.M., De Boer D.K.G., Debije M.G. (2012) Monocrystalline silicon photovoltaic luminescent solar concentrator with 4.2% power conversion efficiency. *Optical Society of America*, 37(15), 3087-3089.

[14] Ecoinvent Centre 2007 ecoinvent Centre (2007), ecoinvent data v2.0. ecoinvent reports No.1-25, Swiss Centre for Life Cycle Inventories, Dbendorf, 2007, retrieved from: www.ecoinvent.org.

[15] Europe 2020 (2015) Retrieved July 2, 2015, from European Commission, Europe 2020 targets website, http://ec.europa.eu/europe2020/europe-2020-in-a-nutshell/targets/index_en.htm

[16] Fattori V., Melucci M., Ferrante L., Zambianchi M., Manet I., Oberhauser W., Giambastiani G., Frediani M., Giachi G., Camaioni N. (2011) Poly(lactic acid) as a transparent matrix for luminescent solar concentrators: a renewable material for a renewable energy technology. *Energy & Environmental Science*, 4, 2849-2853. doi: 10.1039/c1ee01391b

[17] Friedman P.S., Parent C.R. (1987) Luminescent Solar Concentrator Development. Solar Energy Research Institute, april 1987

[18] Fthenakis V., Kim H. C., Frischknecht R., Raugei M., Sinha P., Stucki M. (2011) Life Cycle Inventories and Life Cycle Assessment of Photovoltaic Systems. International Energy Agency (IEA) PVPS Task 12, Report T12-02:2011

[19] Han E., Choi S., Cha S.W. (2013) Diffused Reflection Performance of Microcellular Foamed Polyethylene Naphthalate. *Polymer-Plastics Technology and Engineering*, 52, 1285-1289 doi: 10.1080/03602559.2012.762021

[20] IINAS (2015, March) Development of the Primary Energy Factor of Electricity Generation in the EU-28 from 2010-2013. Retrieved from http://www.iinas.org/tl_files/iinas/downloads/GEMIS/2015_PEF_EU-28_Electricity_2010-2013.pdf

[21] ITRPV (2013) International Technology Roadmap for Photovoltaic (ITRPV) Results 2012. Fourth Edition, March 2013. Retrieved from www.itrpv.net (25-3-15)

[22] Laleman R., Albrecht J., Dewulf J. (2013) Comparing Various Indicators for the LCA of Residential Photovoltaic Systems. In A. Singh et al. (eds), Life Cycle Assessment of Renewable Energy Sources (pp. 211-239) London, UK: Springer

[23] Rodriguez H., Guerrero I., Koch W., Endrs A.L., Franke D., Hssler C., Kalejs J.P., Mller H.J. (2011). Bulk Crystal Growth and Wafering for PV. In A. Luque & S. Hegedus (Eds.), Handbook of Photovoltaic Science and Engineering (pp. 218-261). West Sussex, UK: John Wiley & Sons Ltd.

[24] Roncali J., Garnier F. (1984) Photon-transport properties of luminescent solar concentrators: Analysis and optimization. *Optical Society of America*, 23(16), 2809-2817

[25] Sahin D. (2014) Modeling Light Propagation in Luminescent Media. Ph.D Thesis, University of California. Retrieved from: https://escholarship.org/uc/item/2kt156gp

[26] Salazar J., Sowlati T. (2008) Life cycle assessment of windows for the North American residential market: Case study. *Scandinavian Journal of forest Research*, 23, 121-132. DOI: 10.1080/02827580801906981

[27] Saraidarov T., Levchenko V., Grabowska A., Borowicz P., Reisfeld R. (2010) Non-self-absorbing materials for Luminescent Solar Concentrators (LSC). *Chemical Physics Letters*, 492, 60-62. doi: 10.1016/j.cplett.2010.03.087

[28] Schmidt H., Burger B., Schmid J. (2011). Power Conditioning for Photovoltaic Power Systems. In A. Luque & S. Hegedus (Eds.), Handbook of Photovoltaic Science and Engineering (pp. 954-983). West Sussex, UK: John Wiley & Sons Ltd.

[29] Seng Lim Y., Kim Lo C., Bee Teh G. (2012) Unsaturated polyester resin blended with MMA as potential host matrix for luminescent solar concentrator. *Renewable Energy*, 45, 156-162. doi:10.1016/j.renene.2012.02.025

[30] Seybold G., Wagenblast G. (1989) New Perylene and Violanthrone Dyestuffs for Fluorescent Collectors. *Dyes and Pigments*, 11, 33-317

[31] Slooff L.H., Bende E.E., Burgers A.R., Budel T., Pravettoni M., Kenny R.P., Dunlop E.D., Bchtemann A. (2008) A luminescent solar concentrator with 7.1% power conversion efficiency. *Physical State Solids*, 2, 257-259. doi: 10.1002/pssr.200802186

[32] Tobis I., Caizo del C., Alonso J. (2011). Crystalline Silicon Solar Cells and Modules. In A. Luque & S. Hegedus (Eds.), Handbook of Photovoltaic Science and Engineering (pp. 265-308). West Sussex, UK: John Wiley & Sons Ltd.

[33] Whitaker C.M., Townsend T.U., Razon A., Hudson R.M., Vallv X. (2011). PV Systems. In A. Luque & S. Hegedus (Eds.), Handbook of Photovoltaic Science and Engineering (pp. 814-892). West Sussex, UK: John Wiley & Sons Ltd.

[34] Wilson L.R., (2010) Luminescent Solar Concentrators: A Study of Optical Properties, Re-Absorption and Device Optimisation. Edinburg, UK: Heriot-Watt University;Depertmant of Mechanical Engineering

[35] Wilson L.R., Rowan B.C., Robertson N., Moudam O., Jones A.C., Richards B.S. (2010) Characterization and reduction of reabsorption losses in luminescent solar concentrators. *Optical Society of America*, 49(9), 1651-1661

[36] Yuan Y., Krger. (2012) Polymer-Nanocrystal Hybrid Materials for Light Conversion Applications. *Polymers*, 4, 1-19. doi:10.3390/polym4010001

[37] Xakalashe B.S., Tangstad M. (2011) Silicon processing: from quartz to crystalline silicon solar cells. Southern African Pyrometallurgy Conference, June 6th - 9th, 2011, Johannesburg, South Africa

[38] Xie R., Kolb U., Basch T., Mews A. (2005) Synthesis and Characterization of Highly Luminescent CdSe-Core CdS/Zn05Cd05S/ZnS Multishell Nanocrystals. *Journal of American Chemical Society*, 127, 7480-7488. doi: 10.1021/ja042939g

[39] Youtsey C., Adams J., Chan R., Elarde V., Hillier G., Osowski M., McCallum D., Miyamoto H., Pan N., Stender C., Tatavarti R., Tuminello F., Wibowo A. (2012) Epitaxial Lift-Off of Large-Area GaAs Thin-Film Multi-Junction Solar Cells. CS MANTEC Conference, April 23rd - 26th, 2012, Boston, Massachusetts, USA.

[40] Yue D., You F., Darling S.B. (2014) Domestic and overseas manufacturing scenarios of silicon-based photovoltaics: Life cycle energy and environmental comparative analysis. *Solar Energy*, 105, 669-678. doi: 10.1016/j.solener.2014.04.008

Appendix A

SimaPro input module configuration #1

Table A.1: Material requirements to produce Perylene Perinone

Input	**Quantity**
Methanol, at regional storage/CH S	178.64 g
Water, ultrapure, at plant/GLO S	2164.4 g
Hydrochloric acid, from the reaction of hydrogen with chlorine, at plant/RER S	18 g
Potassium carbonate, at plant/GLO S	5.51 g
N-methyl-2-pyrrolidone, at plant/RER S	93.3 g
Output	**Quantity**
Perylene Perinone	3.0208 g

Table A.2: Material requirements to produce LSC #1 (no cell)

Input	**Quantity**
Polycarbonate granulate (PC), production mix, at plant RER	7680 g
Chemicals organic, at plant/GLO S	3.3536 g
Perylene Perinone	3.0208 g
Injection moulding/RER S	7680 g
Output	**Quantity**
LSC #1 (no cell)	0.64 m^2

Table A.3: Material requirements to produce LSC #1 (cells 5)

Input	**Quantity**
LSC #1 (no cell)	0.64 m^2
Polyethylene terephthalate, granulate, amorphous, at plant/RER S	883.2 g
Polymethyl methacrylate, beads, at plant/RER S	307.2 g
Methyl acrylate, at plant/GLO S	512 g
Photovoltaic cell, single-Si, at plant/RER S	2560 cm^2
Output	**Quantity**
LSC #1 (cells 5)	0.64 m^2

Table A.4: Material requirements to produce LSC #1 (cells 20.75)

Input	**Quantity**
Polyethylene terephthalate, granulate, amorphous, at plant/RER S	1142.7 g
Polymethyl methacrylate, beads, at plant/RER S	79.68 g
Methyl acrylate, at plant/GLO S	132.8 g
Photovoltaic cell, single-Si, at plant/RER S	664 cm^2
LSC #1 (no cell)	0.8281 m^2
Output	**Quantity**
LSC #1 (cells 20.75)	0.8281 m^2

Table A.5: Material requirements to produce LSC #1 (cells 47)

Input	**Quantity**
Polyethylene terephthalate, granulate, amorphous, at plant/RER S	1219.3 g
LSC #1 (no cell)	0.0.8836 m^2
Polymethyl methacrylate, beads, at plant/RER S	45.12 g
Methyl acrylate, at plant/GLO S	75.2 g
Photovoltaic cell, single-Si, at plant/RER S	376 cm^2
Output	**Quantity**
LSC #1 (cells 47)	0.8836 m^2

Table A.6: Material requirements to produce LSC #1 (module 5)

Input	**Quantity**
LSC #1 (cells 5)	0.64 m^2
Aluminium, production mix, wrought alloy, at plant/RER S	11.9 kg
Solar glass, low-iron, at regional storage/RER S	9751.2 g
Flat glass, coated, at plant/RER S	6400 g
Copper, at regional storage/RER S	458.75 g
Section bar extrusion, aluminium/RER S	11.9 kg
Output	**Quantity**
LSC #1 (module 5)	1 m^2

Table A.7: Material requirements to produce LSC #1 (module 20.75)

Input	**Quantity**
LSC #1 (cells 20.75)	0.8281 m^2
Aluminium, production mix, wrought alloy, at plant/RER S	3.85 kg
Solar glass, low-iron, at regional storage/RER S	12421.5 g
Flat glass, coated, at plant/RER S	8281 g
Copper, at regional storage/RER S	229.38 g
Section bar extrusion, aluminium/RER S	3.85 kg
Output	**Quantity**
LSC #1 (module 20.75)	1 m^2

Table A.8: Material requirements to produce LSC #1 (module 47)

Input	**Quantity**
LSC #1 (cells 47)	0.8836 m^2
Aluminium, production mix, wrought alloy, at plant/RER S	2.1 kg
Solar glass, low-iron, at regional storage/RER S	13254 g
Flat glass, coated, at plant/RER S	8836 g
Copper, at regional storage/RER S	115 g
Section bar extrusion, aluminium/RER S	2.1 kg
Output	**Quantity**
LSC #1 (module 47)	1 m^2

Appendix B

SimaPro input module configuration #2

Table B.1: Material requirements to produce GaAs cell (4.3 m_2)

Input	**Quantity**
Water, cooling, unspecified natural origin/kg	77000 kg
Aluminium, primary, at plant/RER S	1.8 kg
Ammonia, liquid, at regional storehouse/RER S	12 kg
Chemicals inorganic, at plant/GLO S	3.1 kg
Chemicals organic, at plant/GLO S	26 kg
Gallium, semiconductor-grade, at plant/GLO S	0.34 kg
Solar glass, low-iron, at regional storage/RER S	88 kg
Hydrogen, liquid, at plant/RER S	12 kg
Hydrochloric acid, from the reaction of hydrogen with chlorine, at plant/RER S	3.4 kg
Hydrogen fluoride, at plant/GLO S	2.2 kg
Indium, at regional storage/RER S	0.015 kg
Nitrogen, liquid, at plant/RER S	4.4 kg
Phosphorus, white, liquid, at plant/RER S	0.037 kg
Silver, at regional storage/RER S	0.19 kg
Sodium chloride, powder, at plant/RER S	0.029 kg
Sodium hydroxide (concentrated) E	2.7 kg
Solvents, organic, unspecified, at plant/GLO S	5.1 kg
Sulphuric acid, liquid, at plant/RER S	1.5 kg
Tap water, at user/RER S	100 kg
De-ionised water, reverse osmosis, production mix, at plant, from groundwater RER S	330 kg
Arsine, at plant/GLO S	2.9 kg
Heat, unspecific, in chemical plant/RER S	7.9 GJ
Output	**Quantity**
GaAs cell	4.3 m_2

Table B.2: Material requirements to produce LSC #2 (no cell)

Input	**Quantity**
Polymethyl methacrylate, sheet, at plant/RER S	3840 g
Injection moulding/RER S	3840 g
Output	**Quantity**
LSC #2 (no cell)	0.64 m^2

Table B.3: Material requirements to produce LSC #2 (cells 5)

Input	**Quantity**
Methyl acrylate, at plant/GLO S	256 g
Polyethylene terephthalate, granulate, amorphous, at plant/RER S	883.2 g
LSC #2 (no cell)	0.64 m^2
GaAs cell	640 cm^2
Output	**Quantity**
LSC #2 (cells 5)	0.64 m^2

Table B.4: Material requirements to produce LSC #2 (cells 20.75)

Input	**Quantity**
LSC #2 (no cell)	0.8281 m^2
Polyethylene terephthalate, granulate, amorphous, at plant/RER S	1142.7 g
Methyl acrylate, at plant/GLO S	66.4 g
GaAs cell	166 cm^2
Output	**Quantity**
LSC #2 (cells 20.75)	0.8281 m^2

Table B.5: Material requirements to produce LSC #2 (cells 47)

Input	**Quantity**
Methyl acrylate, at plant/GLO S	37.6 g
Polyethylene terephthalate, granulate, amorphous, at plant/RER S	1219.3 g
LSC #2 (no cell)	0.8836 m^2
GaAs cell	94 cm^2
Output	**Quantity**
LSC #2 (cells 47)	0.8836 m^2

Table B.6: Material requirements to produce LSC #2 (module 5)

Input	**Quantity**
LSC #2 (cells 5)	0.64 m^2
Aluminium, production mix, wrought alloy, at plant/RER S	11.9 kg
Solar glass, low-iron, at regional storage/RER S	9715.2 g
Flat glass, coated, at plant/RER S	6400 g
Copper, at regional storage/RER S	458.75 g
Section bar extrusion, aluminium/RER	11.9 kg
Output	**Quantity**
LSC #2 (module 5)	1 m^2

Table B.7: Material requirements to produce LSC #2 (module 20.75)

Input	**Quantity**
LSC #2 (cells 20.75)	0.8281 m^2
Aluminium, production mix, wrought alloy, at plant/RER S	3.85 kg
Solar glass, low-iron, at regional storage/RER S	12421.5 g
Flat glass, coated, at plant/RER S	8281 g
Copper, at regional storage/RER S	229.38 g
Section bar extrusion, aluminium/RER	3.85 kg
Output	**Quantity**
LSC #2 (module 20.75)	1 m^2

Table B.8: Material requirements to produce LSC #2 (module 47)

Input	**Quantity**
LSC #2 (cells 47)	0.8836 m^2
Aluminium, production mix, wrought alloy, at plant/RER S	2.1 kg
Solar glass, low-iron, at regional storage/RER S	13254 g
Flat glass, coated, at plant/RER S	8836 g
Copper, at regional storage/RER S	115 g
Section bar extrusion, aluminium/RER	2.1 kg
Output	**Quantity**
LSC #2 (module 47)	1 m^2

Appendix C

SimaPro input module configuration #3

Table C.1: Material requirements to produce LSC #3 (cells 5)

Input	**Quantity**
LSC #2 (no cell)	0.64 m^2
Polyethylene terephthalate, granulate, amorphous, at plant/RER S	883.2 g
Methyl acrylate, at plant/GLO S	1024 g
GaAs cell	376 cm^2
Output	**Quantity**
LSC #3 (cells 5)	2560 m^2

Table C.2: Material requirements to produce LSC #3 (cells 20.75)

Input	**Quantity**
LSC #2 (no cell)	0.8281 m^2
Polyethylene terephthalate, granulate, amorphous, at plant/RER S	1142.7 g
Methyl acrylate, at plant/GLO S	265.6 g
GaAs cell	664 cm^2
Output	**Quantity**
LSC #3 (cells 20.75)	0.8281 m^2

Table C.3: Material requirements to produce LSC #3 (cells 47)

Input	**Quantity**
LSC #2 (no cell)	0.8836 m^2
Polyethylene terephthalate, granulate, amorphous, at plant/RER S	1219.3 g
Methyl acrylate, at plant/GLO S	150.4 g
GaAs cell	376 cm^2
Output	**Quantity**
LSC #3 (cells 47)	0.8836 m^2

Table C.4: Material requirements to produce LSC #3 (module 5)

Input	**Quantity**
LSC #3 (cells 5)	0.64 m^2
Aluminium, production mix, wrought alloy, at plant/RER S	11.9 kg
Solar glass, low-iron, at regional storage/RER S	9715.2 g
Flat glass, coated, at plant/RER S	6400 g
Copper, at regional storage/RER S	1835 g
Section bar extrusion, aluminium/RER S	11.9 kg
Output	**Quantity**
LSC #3 (module 5)	1 m^2

Table C.5: Material requirements to produce LSC #3 (module 20.75)

Input	**Quantity**
LSC #3 (cells 20.75)	0.8281 m^2
Aluminium, production mix, wrought alloy, at plant/RER S	3.85 kg
Solar glass, low-iron, at regional storage/RER S	12421.5 g
Flat glass, coated, at plant/RER S	8281 g
Copper, at regional storage/RER S	917.52 g
Section bar extrusion, aluminium/RER S	9.85 kg
Output	**Quantity**
LSC #3 (module 20.75)	1 m^2

Table C.6: Material requirements to produce LSC #3 (module 47)

Input	**Quantity**
LSC #3 (cells 47)	0.8836 m^2
Aluminium, production mix, wrought alloy, at plant/RER S	2.1 kg
Solar glass, low-iron, at regional storage/RER S	13245 g
Flat glass, coated, at plant/RER S	8836 g
Copper, at regional storage/RER S	115 g
Section bar extrusion, aluminium/RER S	2.1 kg
Output	**Quantity**
LSC #3 (module 47)	1 m^2

Appendix D

SimaPro input module configuration #4

Table D.1: Material requirements to produce QDs

Input	**Quantity**
Oxygen, in air	0.845 g
Cadmium, primary, at plant/GLO S	8.326 g
Selenium, at plant/RER S	45 mg
Methanol, at regional storage/CH S	163.37 g
Toluene, liquid, at plant/RER S	308.94 g
Zinc oxide, at plant/RER S	4.005 g
Fatty acids, from vegetarian oil, at plant/RER S	365.04 g
Zinc, primary, at regional storage/RER S	1.422 g
Hexane, at plant/RER S	6.6 g
Chemicals organic, at plant/GLO S	949.35 g
Output	**Quantity**
QDs	3g

Table D.2: Material requirements to produce LSC #4 (no cell)

Input	**Quantity**
QDs	3 g
Ethylene glycol, at plant/RER S	298.56 g
Methyl acrylate, at plant/GLO S	827.7
Methyl methacrylate, at plant/RER S	4454.4
Injection moulding/RER S	5580.8 g
Output	**Quantity**
LSC #4 (no cell)	0.64 m^2

Table D.3: Material requirements to produce LSC #4 (cells 5)

Input	**Quantity**
LSC #4 (no cell)	0.64 m^2
Photovoltaic cell, multi-Si, at plant/RER S	1280 cm^2
Methyl acrylate, at plant/GLO S	256 g
Output	**Quantity**
LSC #4 (cells 5)	0.64 m^2

Table D.4: Material requirements to produce LSC #4 (cells 20.75)

Input	**Quantity**
LSC #4 (no cell)	0.8281 m^2
Photovoltaic cell, multi-Si, at plant/RER S	332 cm^2
Methyl acrylate, at plant/GLO S	66.4 g
Output	**Quantity**
LSC #4 (cells 20.75)	0.8281 m^2

Table D.5: Material requirements to produce LSC #4 (cells 47)

Input	**Quantity**
LSC #4 (no cell)	0.8836 m^2
Photovoltaic cell, multi-Si, at plant/RER S	188 cm^2
Methyl acrylate, at plant/GLO S	37.6 g
Output	**Quantity**
LSC #4 (cells 47)	0.8836 m^2

Table D.6: Material requirements to produce LSC #4 (module 5

Input	**Quantity**
LSC #4 (cells 5)	0.64 m^2
Aluminium, production mix, wrought alloy, at plant/RER S	11.9 kg
Solar glass, low-iron, at regional storage/RER S	9715.2 g
Flat glass, coated, at plant/RER S	6400 g
Copper, at regional storage/RER S	1835 g
Section bar extrusion, aluminium/RER S	11.9 kg
Output	**Quantity**
LSC #4 (module 5)	1 m^2

Table D.7: Material requirements to produce LSC #4 (module 20.75

Input	**Quantity**
LSC #4 (cells 20.75)	0.8281 m^2
Aluminium, production mix, wrought alloy, at plant/RER S	3.85 kg
Solar glass, low-iron, at regional storage/RER S	12421.5 g
Flat glass, coated, at plant/RER S	8281 g
Copper, at regional storage/RER S	917.52 g
Section bar extrusion, aluminium/RER S	9.85 kg
Output	**Quantity**
LSC #4 (module 20.75)	1 m^2

Table D.8: Material requirements to produce LSC #4 (module 47

Input	**Quantity**
LSC #4 (cells 47)	0.8836 m^2
Aluminium, production mix, wrought alloy, at plant/RER S	2.1 kg
Solar glass, low-iron, at regional storage/RER S	13254 g
Flat glass, coated, at plant/RER S	8836 g
Copper, at regional storage/RER S	115 g
Section bar extrusion, aluminium/RER S	2.1 kg
Output	**Quantity**
LSC #4 (module 47)	1 m^2

Appendix E

SimaPro input inverter and copper wiring

Table E.1: Material requirements to produce copper cable

Input	**Quantity**
Copper, at regional storage/RER S	0.182 kg
Wire drawing, copper/RER S	0.182 kg
Output	**Quantity**
Copper cable	1 m

Table E.2: Material requirements to produce inverter (500W)

Input	**Quantity**
Electricity, medium voltage, production UCTE, at grid/UCTE S	4.24 kWh
Aluminium, production mix, cast alloy, at plant/RER S	0.682 kg
Copper, at regional storage/RER S	0.002 kg
Steel, low-alloyed, at plant/RER S	0.078 kg
Acrylonitrile-butadiene-styrene copolymer, ABS, at plant/RER S	0.148 kg
Polycarbonate, at plant/RER S	0.068 kg
Polyethylene, HDPE, granulate, at plant/RER S	0.014 kg
Styrene-acrylonitrile copolymer, SAN, at plant/RER S	0.002 kg
Polyvinylchloride, at regional storage/RER S	0.002 kg
Printed wiring board, through-hole, at plant/GLO S	0.0596 m^2
Transformer, high voltage use, at plant/GLO S	0.31 kg
Connector, clamp connection, at plant/GLO S	0.005 kg
Inductor, ring core choke type, at plant/GLO S	0.074 kg
Integrated circuit, IC, logic type, at plant/GLO S	0.006 kg
Transistor, wired, small size, through-hole mounting, at plant/GLO S	0.008 kg
Diode, glass-, through-hole mounting, at plant/GLO S	0.02 kg
Capacitor, film, through-hole mounting, at plant/GLO S	0.072 kg
Capacitor, electrolyte type, ¿ 2cm height, at plant/GLO S	0.054 kg
Capacitor, Tantalum-, through-hole mounting, at plant/GLO S	0.0048 kg
Resistor, metal film type, through-hole mounting, at plant/GLO S	0.001 kg
Sheet rolling, steel/RER S	0.078 kg
Wire drawing, copper/RER S	0.002 kg
Section bar extrusion, aluminium/RER S	0.682 kg
Output	**Quantity**
Inverter (500W)	1 p